Journal of Nanobiotechnology

RESEARCH

Open Access

Effectively alleviate rheumatoid arthritis via maintaining redox balance, inducing macrophage repolarization and restoring homeostasis of fibroblast-like synoviocytes by metformin-derived carbon dots

Rui Zhang[1], Xingyu Lin[1], Rongjie Lin[1], Zhenbin Chen[1], Chenfang Miao[2], Yao Wang[2], Xiaoqin Deng[2], Jianlong Lin[3], Shishui Lin[3*], Shaohuang Weng[2*] and Min Chen[1*]

Abstract

Overproduction of reactive oxygen species (ROS), elevated synovial inflammation, synovial hyperplasia and fibrosis are the main characteristic of microenvironment in rheumatoid arthritis (RA). Macrophages and fibroblast-like synoviocytes (FLSs) play crucial roles in the progression of RA. Hence, synergistic combination of ROS scavenging, macrophage polarization from pro-inflammatory M1 phenotype towards M2 anti-inflammatory phenotype, and restoring homeostasis of FLSs will provide a promising therapeutic strategy for RA. In this study, we successfully synthesized metformin-derived carbon dots (MCDs), and investigated the antirheumatic effect in vivo and in vitro. Designed MCDs could target inflamed cells and accumulate at the inflammatory joints of collagen-induced arthritis (CIA) rats. In vivo therapeutic investigation suggested that MCDs reduced synovial inflammation and hyperplasia, ultimately prevented cartilage destruction, bone erosion, and synovial fibrosis in CIA rats. In addition, MCDs eliminated the cellular ROS in M1 phenotype macrophages in RA microenvironment through the enzyme-like catalytic activity as well as inhibiting NOD-like receptor family, pyrin domain containing 3 (NLRP3) inflammasome signaling pathway, effectively polarizing them into the M2 phenotype to realize the anti-inflammatory effect. Furthermore, MCDs could inhibit the proliferation, migration, and fibrosis of inflamed FLSs. Mechanistically, MCDs restored the homeostasis of FLSs while reducing the level of synovial inflammation by blocking IL-6/gp130 signaling pathway. Combined with preferable biocompatibility, MCDs offer a prospective treatment approach for RA.

*Correspondence:
Shishui Lin
linshishuil@fjmu.edu.cn
Shaohuang Weng
shweng@fjmu.edu.cn
Min Chen
chenminfz006@163.com

Full list of author information is available at the end of the article

Keywords Metformin-derived carbon dots, Treating rheumatoid arthritis, Redox balance, Macrophage repolarization, Fibroblast-like synoviocytes, IL-6/gp130 signaling pathway

Introduction

Rheumatoid arthritis (RA) is a common chronic autoimmune disorder with an adult incidence of 0.5-1% worldwide, posing an enormous burden and challenge to global public health [1, 2]. Characterized by persistent synovium inflammation as well as cartilage and bone destruction, RA may eventually lead to irreparable joint functional disability without proper therapeutic intervention [3, 4]. Unfortunately, the clinical management effect of RA remains unsatisfied due to its elusive pathogenesis. Current medicine treatment involved: non-steroidal anti-inflammatory drugs (NSAIDs), disease-modifying anti-rheumatic drugs (DMARDs), glucocorticoids, and biologicals (adalimumab, rituximab, etc.) [5–7]. However, their pharmacological action only concentrates on some simple pathological processes and associated with various side effects (gastrointestinal ulcer, liver/kidney damage, osteoporosis, osteonecrosis, etc.). There is an urgent need to develop a safe and efficient treatment candidate for RA.

Accumulating evidence indicates that macrophages mainly participate in the pathogenesis and progression of RA due to its high infiltration in joint synovium [8, 9]. Macrophages with M1 phenotype play a pivotal role in the secretion of pro-inflammatory cytokines including interleukin 1β (IL-1β), interleukin 6 (IL-6), and tumor necrosis factor (TNF-α) to promote the development of inflammation. On the contrary, M2 macrophages secrete anti-inflammatory cytokines such as interleukin 4 (IL-4) and interleukin 10 (IL-10) for the relief of inflammation. In RA joints, M1 macrophages are the predominant phenotype with an abnormal increase of M1/M2 ratio with the overexpression of pro-inflammatory cytokines [10, 11]. Sustained secretion of inflammatory cytokines not only aggravate synovitis, but also cause the erosion of cartilage and bone [12, 13]. Meanwhile, the high level of oxidative stress is closely related to the inflammation progression in RA [14]. Activated NOD-like receptor family, pyrin domain containing 3 (NLRP3) inflammasome widely participates in systematic and local inflammation in RA [15]. Overproduction of reactive oxygen species (ROS) can trigger the generation of inflammatory cytokines by activating NLRP3 inflammasome signaling pathway [16, 17]. Simultaneously, pro-inflammatory cytokines may amplify the production of ROS which result in accelerating the disorder process [18, 19]. Hence, scavenging overproducted ROS and reprogramming M1 macrophages to M2 macrophages will prevent RA associated joint inflammation and damage. However, suppression of the proinflammatory cytokines and antioxidant therapy cannot result in the complete cure of RA [20], suggesting that RA is also influenced by other factors that are not addressed by current treatment [21].

Besides macrophages, fibroblast-like synoviocytes (FLSs) are crucial cells in RA. Aggressive phenotype FLSs can lead to several inflammation, cartilage, and bone destruction via released pro-inflammatory cytokines and matrix metalloproteinase [22, 23]. Under repeated inflammatory stimulation, FLSs secrete extracellular matrixes components such as collagen I (Col-I) and α-smooth muscle actin (α-SMA), which eventually contribute to fibrosis [24]. Synovial fibrosis is conformed related to the clinical symptoms of pain and stiffness, together with synovitis and abnormal proliferation deteriorated RA [25, 26]. Recent research points out that reducing synovial inflammation levels could block IL-6/gp130 signaling pathway to inhibit FLSs proliferation, migration, and fibrosis with treating effect on RA [27]. Thus, a therapy that controls the enhanced generation of ROS and pro-inflammatory cytokines, restoring FLSs homeostasis is a promising therapeutic choice for RA.

Methotrexate (MTX), one of DMARDs, is the first-line drugs for RA. Though the high-dose treatment with MTX achieves an optimistic therapeutic efficacy, it inevitably exists poor target therapy and adverse reactions [28, 29]. With the development of nanomedicine, nanomaterials with immunoregulation or antioxidant ability have been gradually designed and constructed in the treatment of RA and other inflammatory diseases [30–32]. Nanomaterials with specific particle size pass through the blood vessels and accumulate in the inflammation joint through the mechanism of passive targeting which called extravasation through leaky vasculature and subsequent inflammatory cell-mediated sequestration (ELVIS) effect [33, 34]. A variety of nanomaterials have been developed and loaded with specific drugs as nano-delivery platform for the treatments of RA [35–37]. Although nanomedical drugs have unlimited potentials, reasonable intervention has not been realized to treat RA in terms of ROS clearance, M1/M2 regulation and FLSs improvement in RA microenvironment, and the prospect of therapeutic effect is still unknown and lack. Carbon dots (CDs), a new zero-dimensional carbon-based nanomaterial, exhibit preferable biocompatibility and adjustable biological capabilities [38, 39]. Through optimization of preparation materials, reaction conditions and post-treatment methods, CDs with specific structural differences and functional modifications can be obtained for the diagnosis and treatment of various diseases [40–42]. In our previous works, some kinds of CDs were synthesized by appropriate materials

and preparation strategies for the achievement of the antibacterial ability [41, 43] and antioxidant activity [44]. Nevertheless, the ROS scavenging capability of CDs might be insufficient to realize the favorable immunoregulation and to inhibit the proliferation, migration, and fibrosis of FLSs for treating RA. As a classical oral biguanides drug, metformin has been widely adopted in treating diabetic mellitus. In addition to reduce the level of blood glycemia, series researches verify that metformin is correlated with some other effects of bone regeneration and anti-inflammation [45–47]. Resultantly, we propose that a certain kind of CDs using metformin as one of the sources could efficiently introduce extraordinary capabilities besides antioxidant ability for potentially treating RA.

In this work, we designed and synthesized metformin-derived carbon dots (MCDs) through a one-step hydrothermal method using anhydrous citric acid (CA), ethane diamine (EDA), and metformin. We investigated the therapeutic effects and mechanism of MCDs on RA (Scheme 1). MCDs were uptaken by macrophages and FLSs, and targeted inflammation joint in collagen-induced arthritis (CIA) rats. As a result, MCDs displayed preferable therapeutic effects as inhabitation of inflammatory, cartilage/bone erosion, FLSs fibrosis in CIA rats as well as favorable biocompatibility in vivo. In vitro study suggested that MCDs could promote macrophages polarization from M1 phenotype to M2 phenotype in both normal and inflammatory environment. Besides, MCDs inhibited the proliferation, migration, inflammation, and fibrosis of FLSs. Mechanistic studies revealed that MCDs could block NLRP3 inflammasome signaling pathway which leads to macrophages immunoregulation through scavenging overproduction of ROS. Furthermore, MCDs downregulated synovium inflammation level to inhibiting FLSs proliferation, migration, and fibrosis by blocking IL-6/gp130 signaling pathway. The mimic-clinical application was conducted using human-derived cells (THP-1 and FLSs isolated from RA patients) to validate the therapeutic effects and mechanism of MCDs. This work develops an effective RA treatment agent based on CDs with a clarified mechanism, suggesting the particular prospect in future clinical treatment.

Results

Characterization of MCDs

The prepared MCDs were comprehensively characterized. Transmission electron microscope (TEM) studies revealed that MCDs were regular monodisperse spherical structure with a particle size distribution between 1.25 and 5.25 nm with the average diameter of 3.26 nm. High-resolution TEM (HRTEM) illustrated a lattice spacing of 0.21 nm, assigned to the graphite (100) plane (Fig. 1A) [48]. The X-ray Diffraction (XRD) analysis of MCDs (Fig. S1) revealed MCDs had a band diffraction peak centered at $2\theta = 28.04°$ and a broad diffraction peak at $2\theta = 42.72°$. The diffraction peak at 28.04° was associated with the (002) crystal plane of graphite, indicative of the typical

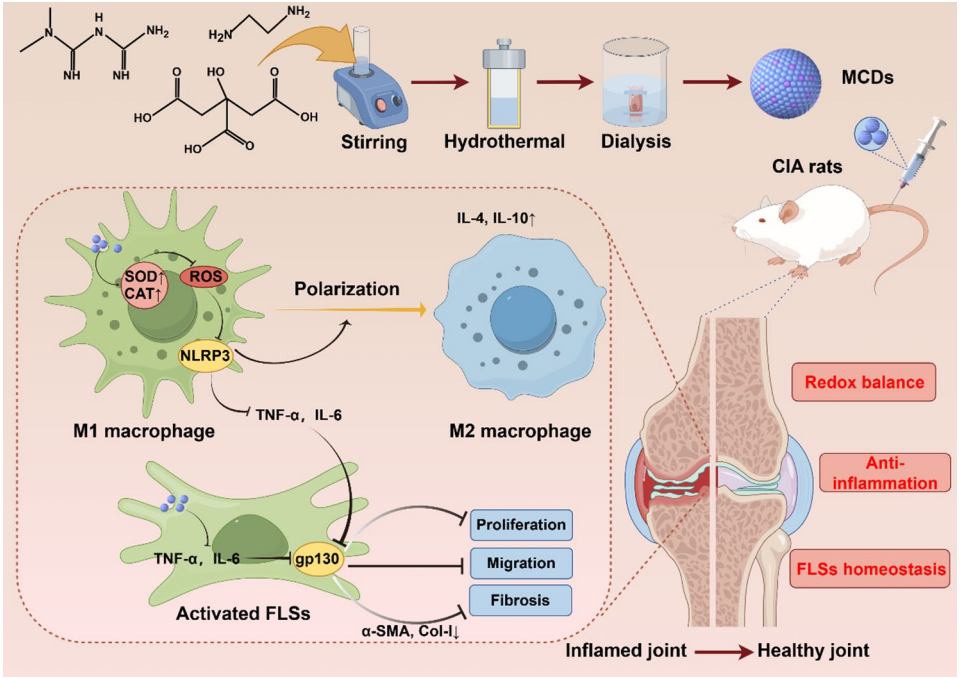

Scheme 1 Schematic illustration of MCDs fabrication and therapeutic mechanism of MCDs against RA. MCDs displayed both ROS scavenging and induced macrophages polarization from pro-inflammatory M1 phenotype to anti-inflammatory M2 phenotype in RA microenvironment. Meanwhile, MCDs regulated the homeostasis of FLSs through inhibiting proliferation, migration, and fibrosis

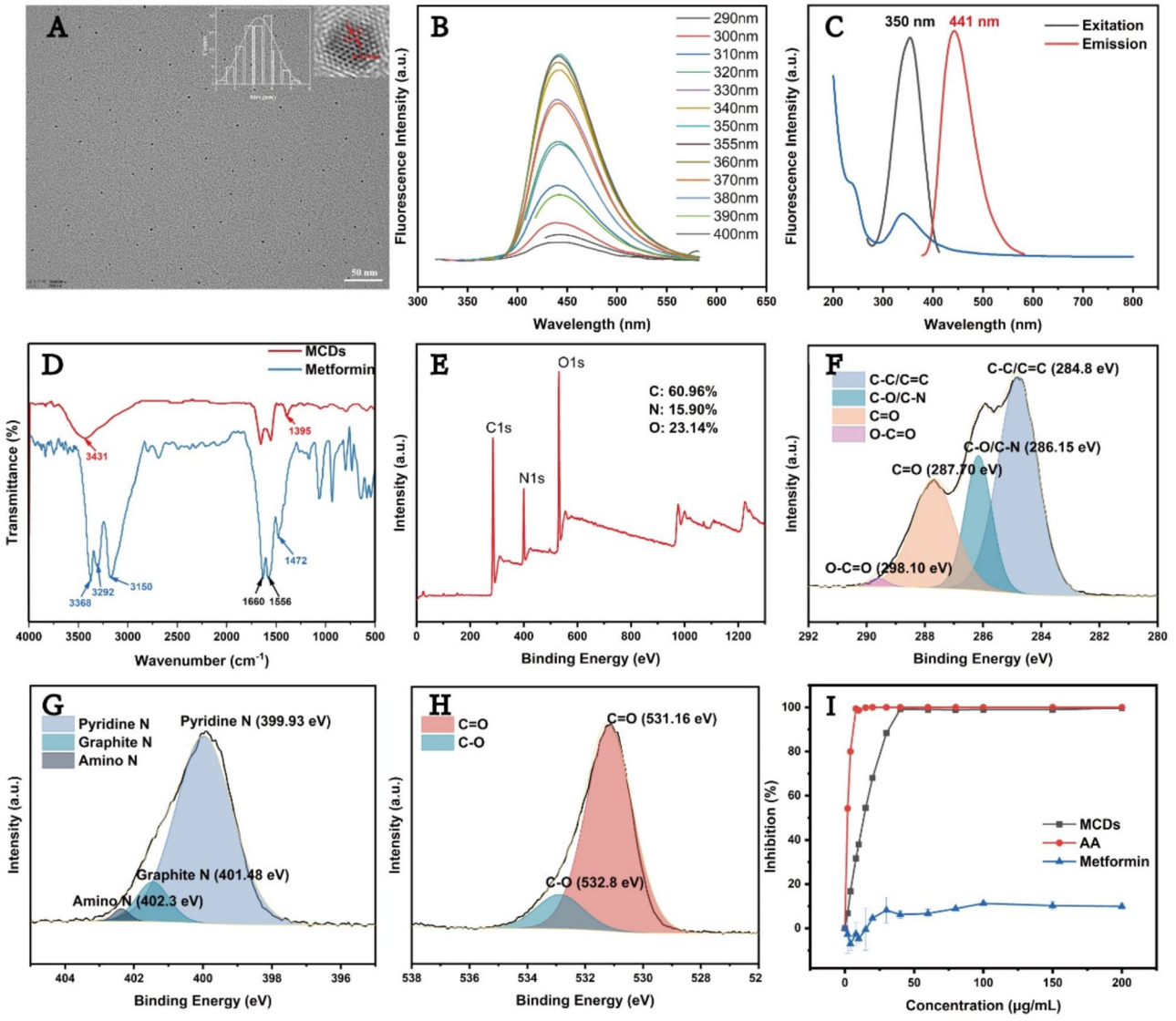

Fig. 1 Characterization of MCDs. (**A**) TEM image with HRTEM and size distribution. (**B**) Fluorescence emission spectra of MCDs at 290–400 nm excitation. (**C**) UV–vis absorbance, maximum exciting, and emission fluorescence spectra. (**D**) FTIR spectra of MCDs and metformin. (**E**-**H**) XPS spectra and high-resolution XPS spectra of C1s, N1s, and O1s. (**I**) ABTS radicals scavenging efficiency of MCDs compared with that of ascorbic acid (AA) and metformin. The values reported are mean ± SD, $n = 6$

interlayer spacing observed in graphitic carbon [49]. The peak at 42.72° was typically attributed to the (100) crystal plane of graphitic-like carbon, signifying atomic ordering within the two-dimensional graphene planes [48]. The results from HRTEM and XRD illustrated the inclusion of carbonized graphitic structures of MCDs. As an important parameter of carbon dots, the optical properties of MCDs were also evaluated. The emission center of MCDs at 440 nm only shifted slightly at variable excitation wavelengths from 290 to 400 nm (Fig. 1B), indicating the iconic excitation-independent emission property of carbon dots [50]. Correspondingly, MCDs displayed maximum excitation and emission wavelengths at 350 nm and 441 nm, respectively (Fig. 1C). The absorption spectrum of the MCDs revealed the absorbance peaks at 245 nm and 345 nm, attributed to the π-π* transition of sp^2 hybridization of the C = C bond and n-π* transition of C = O, respectively [51, 52].

The chemical structure of MCDs was investigated. Fourier transform infrared spectrometer (FTIR) result showed the absorption peaks of metformin at 3368 cm^{-1}-3150 cm^{-1}, and 1556 cm^{-1}, which were attributed to the stretching and bending vibrations of the N-H bond. The absorption peaks of 1472 cm^{-1} was attributed to the stretching vibration of C = N bond. The absorption peaks of MCDs at 3431 cm^{-1} was attributed to the stretching vibration of O-H bond, 1395 cm^{-1} was attributed to the stretching vibration of C = N bond,

while 1660 cm^{-1} and 1556 cm^{-1} were attributed to the stretching vibration of C = O and N-H bonds, respectively (Fig. 1D). Three typical peaks of C1s (296.8 eV), N1s (408.8 eV), and O1s (540.8 eV) were observed in X-ray photoelectron spectroscopy (XPS) full-wavelength spectrum of MCDs, with corresponding element percentages of 60.96%, 15.90%, and 23.14%, respectively (Fig. 1E). The high-resolution XPS spectra of C1s showed the four fitting bands of C-C/C = C (284.8 eV), C-O/C-N (286.15 eV), C = O (287.7 eV), and O-C = O (298.1 eV) [53]. Among them, the integral areas of sp^2 hybrid carbon C-C/C = C, sp^2 hybrid carbon O-C = O, sp^3 hybrid carbon C-O/C-N and sp^3 hybrid carbon C = O were accounted to be 51.60%, 0.70%, 25.47% and 22.23% of the total C content of MCDs, respectively (Fig. 1F). Three binding energies of 399.93 eV, 401.48 eV, and 402.3 eV were fitted from high-resolution XPS spectra of N1s, which were derived from pyrrole nitrogen (70.89%), graphite nitrogen (20.32%) and amino nitrogen (8.79%), respectively (Fig. 1G) [54]. The high-resolution XPS spectra of O1s had two fitting bands, indicating that O element mainly existed in the form of C = O (531.16 eV, 76.95%) and C-O (532.8 eV, 23.05%) (Fig. 1H). XPS results indicate that MCDs are successfully doped with N element and the surface of MCDs is rich in electron-donating functional groups. The results of FTIR and XPS indicate that metformin and MCDs have similar functional groups of $-NH_2$ and C = N. While, MCDs display newly functional groups of -OH and C = O, which indicate that raw materials gradually oxidized and polymerized during hydrothermal process. Meanwhile, the presence of $-NH_2$, -OH, and -COOH are the electron-donor groups. NMR was used for further chemical structure characterization of MCDs. The ^{13}C NMR spectrum of metformin exhibited a signal at approximately 160 ppm corresponding to the functional groups of C = N, while 40 ppm related to the methyl carbon ($N-CH_3$). In the ^1H NMR spectrum, the peak at 2–4 ppm corresponded to the functional groups of $N-CH_3$, while the peak at 4.5-6.0 ppm ascribed to the $C-NH_2$ and C = NH (Fig. S2A, S2B) [55]. Correspondingly, the ^{13}C NMR spectrum of MCDs displayed peaks in 20, 40, and 50 ppm associated with sp^3 hybridized aliphatic C atoms in C-C, $N-CH_3$, and C-O bonds, respectively. Peaks within the range of 100–140 ppm were indicated carbonization/nucleation of MCDs with C = C bonds [56]. The region between 160 and 180 ppm in the ^{13}C NMR spectrum was attributed to $C-NH_2$ and amide groups [57]. Furthermore, the peaks within the range of 2–4 ppm in ^1H NMR spectrum of MCDs were the specific functional groups of CH-N, O-H, and N-H (Fig. S2C, S2D). NMR results proved that MCDs had the different structural feature with metformin. Besides, the functional groups of -OH, -COOH, and $-NH_2$ were observed in NMR, which were consistent with the FTIR and XPS characterizations.

The antioxidant activity of MCDs was initially evaluated using the ABTS radical scavenging assay. As the concentration of MCDs increased, the color of the ABTS gradually lightened, indicating the capability of MCDs to scavenge ABTS radicals (Fig. 1I). The ABTS radical scavenging rates revealed that both MCDs and AA exhibited concentration-dependent behavior in scavenging ABTS radicals (Fig. 1I). When MCDs reached a concentration close to 40 μg/mL and AA approached 6 μg/mL, the scavenging efficiencies for ABTS radicals were nearly 100% and then stabilized. The half maximal effective concentration (EC50) values for scavenging ABTS radicals were approximately 14.72 μg/mL for MCDs and 1.99 μg/mL for AA, respectively. In contract, the introduction of 100 μg/mL metformin only exhibited 10.09% scavenging efficiencies for ABTS radicals, suggesting the little antioxidant activity of metformin (Fig. 1I). After dissolved in ultrapure water and stored for one month, MCDs and AA achieved an EC50 of approximately 18.67 μg/mL and 3.12 μg/mL for scavenging ABTS radicals, respectively (Fig. S3A). After three months of storage, these values increased to approximately 23.52 μg/mL for MCDs and 5.17 μg/mL for AA (Fig. S3B), indicating that MCDs have preferable and stable ABTS radical scavenging performance in a long-time period. Considering the fact that superoxide anion ($O_2^{\bullet-}$) and hydrogen peroxide (H_2O_2) play a main role in oxidative stress, the scavenging activities of MCDs towards $O_2^{\bullet-}$ and H_2O_2 were further evaluated. As shown in Fig. S4, MCDs exhibited excellent and concentration-dependent scavenging properties to $O_2^{\bullet-}$ and H_2O_2. According to the structural characterization of MCDs, the presence of electron-donor groups ($-NH_2$, -OH, and -COOH) as well as sp^2/sp^3 hybrid carbon network structure are responsible for the effective ROS scavenging activity and other potential properties [44, 58, 59].

MCDs achieve targeting capability towards RA both in vitro and in vivo

The targeting ability of MCDs towards RA was examined using cellular uptake assay and in vivo animal imaging technique. Macrophages and FLSs are the two primary cell types affected by synovium inflammation in RA. RAW264.7 and FLS (Mouse-derived FLSs) were applied as representative cells for macrophages and FLSs, respectively. Firstly, the accumulation capability of MCDs was assessed by confocal laser scanning microscopy (CLSM) in RAW264.7 and FLS in vitro. CLSM results showed that MCDs gradually accumulated in RAW264.7 both in normal and LPS and IFN-γ (LPS + IFN-γ) simulated inflammatory environments as the incubation time increased (Fig. 2A). The quantitative results of average fluorescence intensity indicated no significant difference

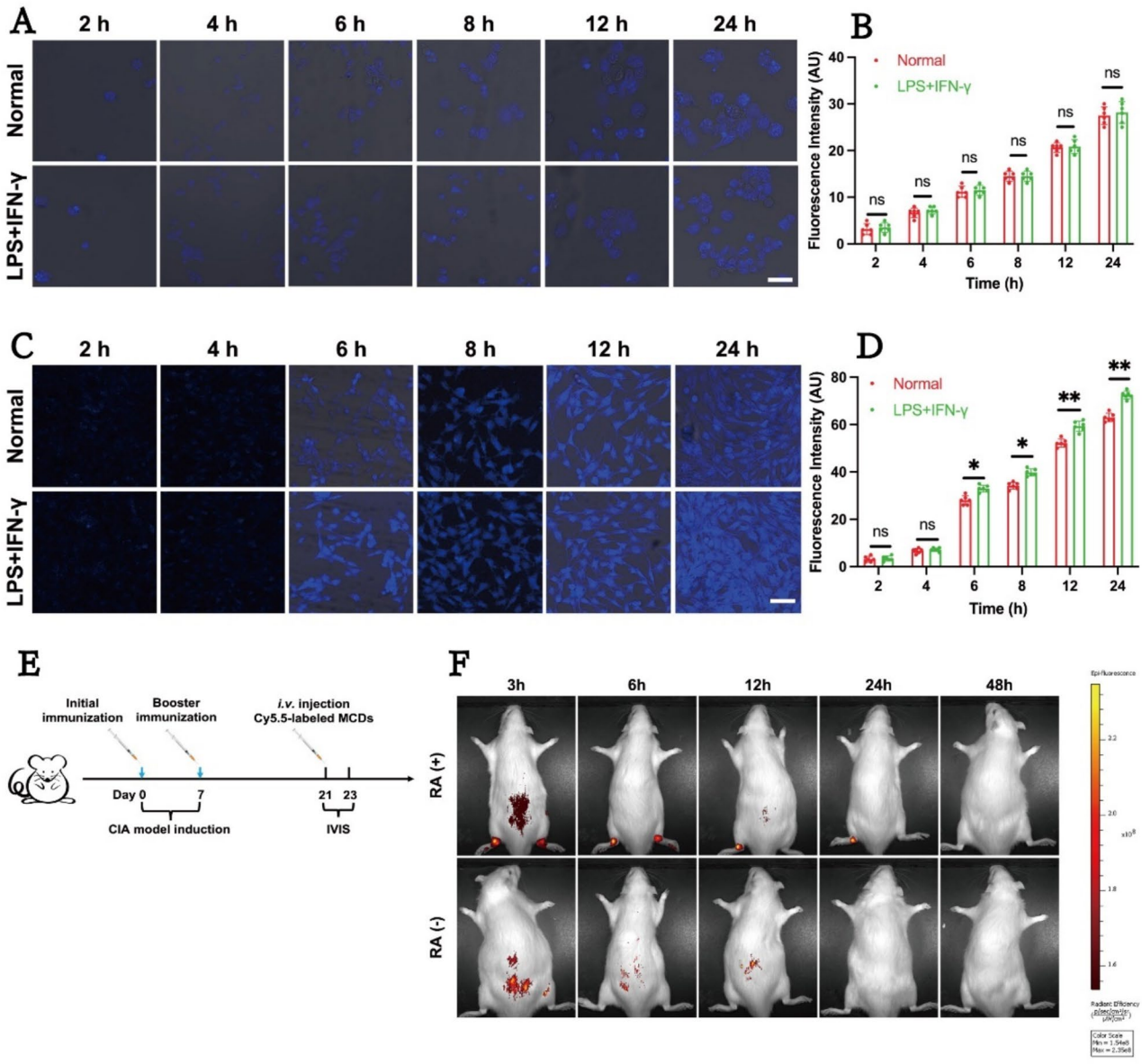

Fig. 2 The in vitro and in vivo targeting capability of MCDs. (**A**) Confocal micrographs of cellular uptaken assay in normal and inflamed RAW264.7 for consecutive period (Blue fluorescence: MCDs, Scar bar = 200 μm). (**B**) Semi-quantitative results of fluorescence intensity from (**A**). The values reported are mean ± SD, $n = 6$. (**C**) Confocal micrographs of cellular uptaken assay in normal and inflamed FLS for consecutive period (Blue fluorescence: MCDs, Scar bar = 200 μm). (**D**) Semi-quantitative results of fluorescence intensity from (**C**). The values reported are mean ± SD, $n = 6$, $^{*}P < 0.05$, $^{**}P < 0.01$, $^{***}P < 0.001$. (**E**) Schematic diagram of biodistribution experiment in vivo. (**F**) Representative images of Cy5.5-MCDs fluorescence in normal and CIA rats after intravenous administration for different time points

between these two environments at different periods (Fig. 2B). As for FLS, MCDs were also be uptaken in both normal and inflammatory environments with the extension of observation time (Fig. 2C). There was no significant difference in the average fluorescence intensity of MCDs uptaken by FLS under different conditions at 2 h and 4 h of incubation (Fig. 2D). However, the average fluorescence intensity of MCDs in LPS + IFN-γ activated FLS was significantly higher than in the normal condition after 6 h of incubation. Above results demonstrate that MCDs can enter RAW264.7 and FLS in both normal and inflammatory environment, while FLS exhibit higher cellular uptake of MCDs than RAW264.7 in the inflammatory environment.

Cy5.5 with a red fluorescence is an effective labeling indicator for tracking distribution of nanoparticles in IVIS system [60]. The label of MCDs using Cy5.5 was characterized and proved by UV-vis absorbance and FTIR spectra (Fig. S5), and related explanation. The successfully combined Cy5.5 and MCDs was introduced for

evaluating the in vivo distribution of MCDs. The in vivo distribution of Cy5.5-MCDs was observed following a single intravenous administration in both CIA and normal rats (Fig. 2E and F). Fluorescence of Cy5.5-MCDs was detected in both groups after 3 h of tail vein injection. In normal rats, the fluorescence of Cy5.5-MCDs was mainly concentrated in the abdominal area, with intensity gradually decreasing between 3 and 12 h and disappearing within 24 h, indicating that the MCDs were mostly cleared from the body through metabolism (Fig. 2F). Nevertheless, Cy5.5-MCDs showed a strong fluorescent signal in the inflamed joints of CIA rats, with the highest accumulation at 3 h post-administration, followed by a gradual decrease over 24 h (Fig. 2F). The red fluorescence from Cy5.5-MCDs was no longer detectable in CIA rats after 48 h, suggesting nearly complete clearance of MCDs from the body. These results together confirm that the synthesized MCDs efficiently and selectively target pro-inflammatory FLSs and achieve remarkably accumulation in inflamed joints of CIA rats. This targeting is facilitated by the ELVIS effect, attributed to the specific particle size and the main inflammatory response caused from cells in the joints of RA [61]. This establishes a solid foundation for the potential treatment of RA.

MCDs inhibit synovium inflammation and fibrosis in CIA rats

Hemolysis test was initially performed to evaluate the in vivo safety of MCDs for tail vein injection. As shown in Fig. S6, almost no hemolysis phenomenon was found with MCDs. The hemolysis rate of red blood cells was less than 5% when the concentration of MCDs ranging from 1 to 1500 μg/mL, indicating that MCDs had low toxicity to red blood cells. It is safe and reliable for MCDs to select appropriate concentration or dose for intravenous injection.

The antirheumatic property of MCDs in CIA rats were extensively examined across different treatment groups (Refer to the "Materials and methods" section in the SI for the grouping method) (Fig. 3A). MTX, the gold standard for clinical RA treatment, was used as a positive drug control. After 21 days of arthritis induction, the paws and ankles of CIA rats showed severe swelling (Fig. S7). MCDs and MTX were then intravenously injected into CIA rats based on the different groups. The body weight, arthritis index, and the paw thickness of each group were measured every three days throughout the study period. Since the initial immunization, the body weight of CIA rats showed a slow growth trend and was significantly lower than that of normal rats. The daily activities of CIA rats were limited and affected seriously due to the local and systemic inflammatory reactions. After intravenous administration of MTX and MCDs, especially high dose of MCDs, the restriction of body weight was relieved (Fig. 3B). Compared to the Healthy group rats, the arthritis index and paw swelling were drastically increased and accompanied by severe inflammation in CIA rats. However, the increase of these signs was slower after the administration of MCDs and MTX. Notably, the arthritis index and paw swelling in MCDs-H group were significantly lower than MCDs-M and MCDs-L group, while showed no significant difference with MTX group (Fig. 3C and D). The impact of MCDs on oxidative stress level in CIA rats was investigated through the detection of tissue superoxide dismutase (SOD) and catalase (CAT) activity. As illustrated in Fig. S8, the activities of SOD and CAT in the CIA group were significantly lower than those in the Healthy group, indicating that there was a higher level of local oxidative stress in the joint tissues of CIA rats. When MCDs were injected into CIA rats via tail vein, the activities of SOD and CAT increased in varying extents. Compared with CIA group, the slightly enhanced SOD and CAT activities were observed in the MCDs-L, and MCDs-M groups (Fig. S8). Whereas, the MCDs-H and MTX groups showed increased SOD and CAT activity compared to the CIA group. The elevated SOD and CAT activity in cellular or tissue suggests a reduction in oxidative stress levels through the scavenging of $O_2^{\bullet-}$ and H_2O_2, respectively [62], thereby confirming the in vivo antioxidant activity of MCDs.

Micro-CT imaging was employed to assess bone erosion in the ankle joints of the six groups (Fig. 3E). The top and bottom figures represented the reconstructed micro-CT images of the ankle joints after one and two weeks of different interventions. Red arrows indicated the areas of bone tissue damage. The Healthy group had smooth bone surfaces, whereas the CIA group showed a rough bone surface and severe bone erosion in the inflamed ankle with significant reduction in bone mineral density (BMD) (Fig. S9). The MCDs-L and MCDs-M groups exhibited reduced levels of bone destruction compared to the CIA group. Unsurprisingly, the MCDs-H and MTX groups resulted in smooth bone surface, favorable relief on bone erosion, and BMD levels approaching those of normal rats. All these data support that MCDs effectively promote the repair of erosive bone in CIA rats.

Histological analysis of rat ankle joints from different groups were conducted (Fig. 3F). H&E-stained sections in CIA group showed a large number of inflammatory cell infiltration and severe synovial hyperplasia (indicated by black arrows). Compared to the CIA group, the MCDs-L and MCDs-M groups showed satisfying improvements in synovium invasion, although some inflammatory cell infiltration persisted. In the MCDs-H and MTX groups, infiltration of inflammatory cell in the synovium had been greatly ameliorated. The joint cavity surfaces in the MCDs-H and MTX groups showed clear boundaries and the minimal synovial hyperplasia, which

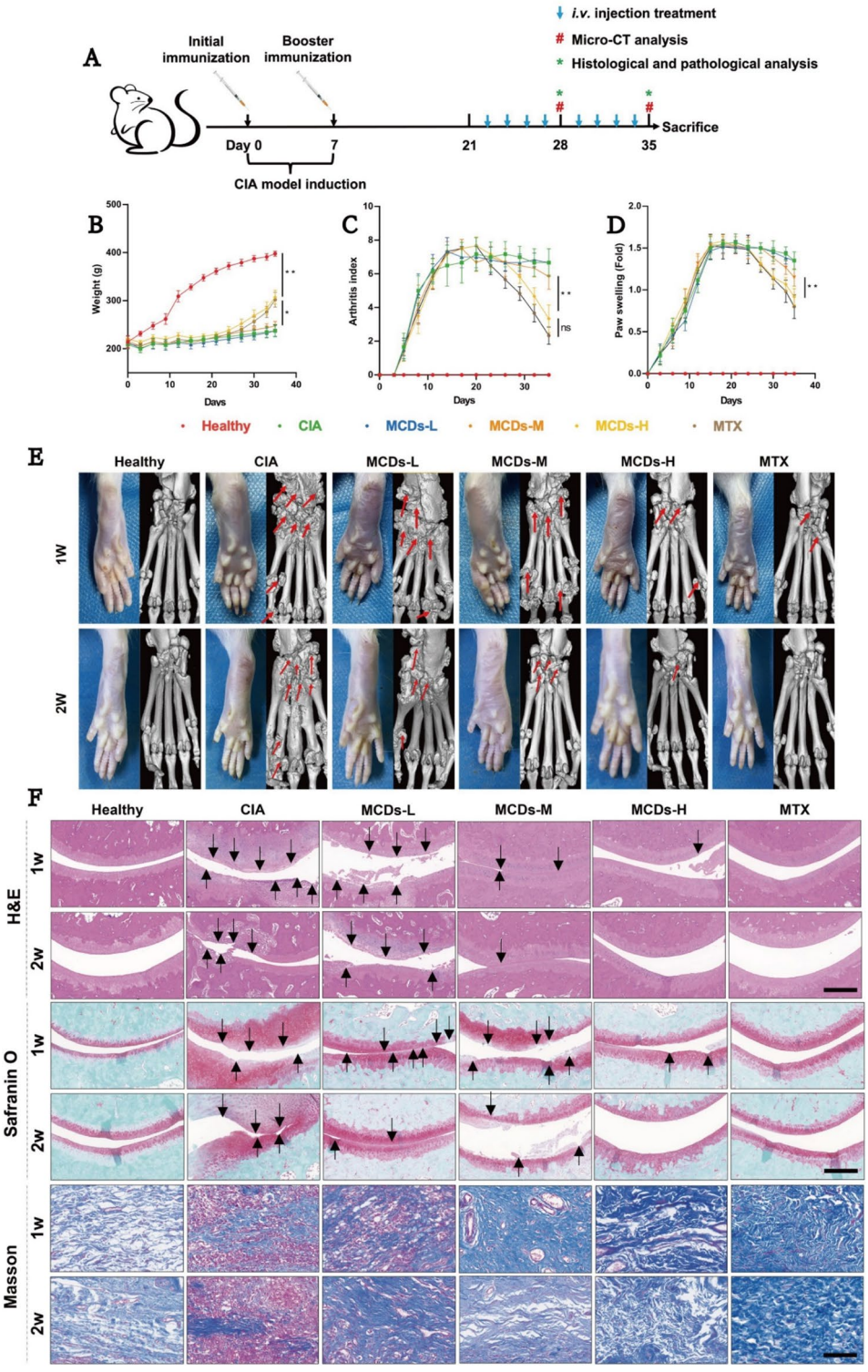

Fig. 3 Therapeutic efficiency of MCDs in CIA rats. (**A**) The schematic illustration of MCDs treatment in CIA rats. (**B**-**D**) The body weight, arthritis index, and paw swelling in different groups during experiment period. The values reported are mean ± SD, $n = 6$, $^{*}P < 0.05$, $^{**}P < 0.01$, $^{***}P < 0.001$. (**E**) Representative images of hindlimbs and micro-CT after one and two weeks of treatment from different groups. (**F**) The H&E, Safranin O, and Masson staining of ankle joints and synovium after one and two weeks of treatment from different groups (Scar bar = 200 μm)

were similar to that in the Healthy group. Safranin-O staining of the ankle joints showed complete destruction of cartilage in the CIA group (black arrows) (Fig. 3F). A portion of cartilage in the MCDs-L and MCDs-M groups was damaged due to synovium invasion, but another portion remained intact. Moreover, cartilage structure of MCDs-H and MTX groups showed more intact and clearer boundaries than that of MCDs-L and MCDs-M groups. Finally, compared with normal rats, Masson staining of synovial tissue revealed that pronounced collagen fiber hyperplasia and deposition (red staining) were observed in CIA group, indicating obviously activation of FLSs and the presence of synovial fibrosis in CIA rats. The area of the red regions was significantly decreased in the MCDs-L and MCDs-M groups, suggesting the certain control of collagen fiber hyperplasia and deposition. Moreover, collagen fiber deposition in the synovial tissue greatly reduced after intravenous injection of MCDs-H and MTX, with the blue fibrosis regions in these groups recovered to a healthy level (Fig. 3F).

Immunohistochemical staining was carried out to indicate the variable inflammation reaction. Compared to normal rats, the upregulated positive expression areas of TNF-α and IL-6 were found in CIA group, while the expression areas of IL-4 and IL-10 were downregulated (Fig. 4A, Fig. S10). Additionally, the expression of

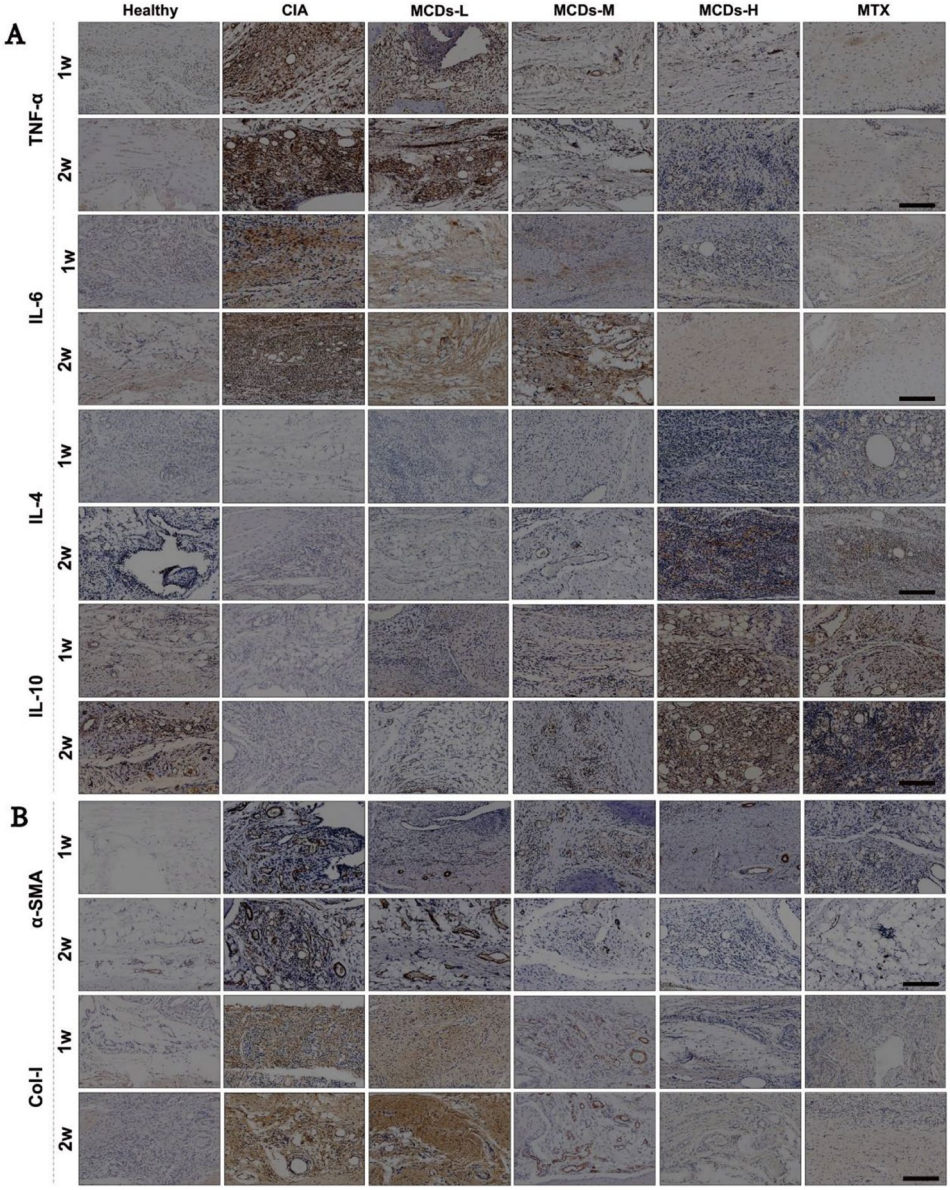

Fig. 4 Immunohistochemical staining images of different indicators in CIA rats for evaluating antirheumatic effect of MCDs. (**A**) The inflammation related indicators of TNF-α, IL-6, IL-4, and IL-10. (**B**) The fibrosis related indicators of α-SMA and Col-I (Scar bar = 200 μm)

these pro-inflammatory cytokines can be reduced as the increased dose of MCDs. Meanwhile, the changed expression of anti-inflammatory cytokines was observed in the MCDs and MTX groups with the opposite pattern of pro-inflammatory cytokines. The levels of TNF-α, IL-6, IL-4, and IL-10 in MCDs-H group were almost similar to the MTX group. Accordingly, the peripheral blood concentrations of TNF-α, IL-6, IL-4, and IL-10 in the all groups were detected. The MCDs treated groups inhibited the expression of pro-inflammatory cytokines (TNF-α, IL-6) and promoted the secretion of anti-inflammatory cytokines (IL-4, IL-10) (Fig. S11), which were consistent with the results of immunohistochemical analysis (Fig. S10). In addition, the expression of fibrosis related indicators (α-SMA and Col-I) were evaluated as well. Compared to the Healthy group, the immunohistochemical images revealed the enhanced expression levels of α-SMA and Col-I in CIA group. Whereas, the α-SMA and Col-I levels were gradually suppressed with the increased dose of MCDs (Fig. 4B, Fig. S12). Among them, MCDs-H and MTX groups showed no significant difference with the Healthy group, confirming the inhibition effect of MCDs on synovial fibrosis.

The in vivo safety of MCDs was further examined by blood biochemistry and H&E staining of the main organs. It can be seen that the ALT and AST levels in the CIA group were higher than that in the Healthy group (Fig. S13). Among all intervention groups, the overall indicators of liver and kidney function decreased in CIA group after MCDs treatment, and showed no significant difference with the Healthy group. While, the levels of ALT, AST, BUN and CREA in the MTX group were significantly higher than those in Healthy group (Fig. S13), implying that long-term systemic administration of MTX could cause damage to liver and kidney to a certain extent. The biochemistry indexes of MCDs-related groups were much lower than those of the MTX group and closed to the Healthy group, indicating that MCDs had little hepatorenal toxicity compared with MTX. In H&E staining, the hepatic sinusoidal hyperemia (black arrows) appeared in the liver of MTX group (Fig. S14), which is considered as the liver injury due to the cytotoxicity of MTX [63]. Abnormal changes and pathological lesions were not observed in MCDs treated and Healthy groups, indicating the favorable biocompatibility of MCDs. Taken together, it deduces that MCDs with in vivo safety exert the in vivo treating effects of the synergistic effects of ROS scavenging capability, immunomodulatory capacity, preventing cartilage/bone destruction, and inhibiting synovial fibrosis.

MCDs display ROS scavenging and macrophages polarization through inhibiting NLRP3 inflammasome signaling pathway

It has been demonstrated that redox homeostasis and the polarization of the macrophage from M1 phenotypes to M2 phenotypes have beneficial therapeutic effects on RA [64]. Given the in vivo ROS scavenging and immunoregulation capabilities of MCDs, the in vitro antioxidant and macrophage polarization effects of MCDs were evaluated. First, RAW264.7 and FLS were selected to evaluate the potential cytotoxicity of MCDs. At high concentrations of 1000 μg/mL, MCDs exhibited minimal cytotoxicity, indicating favorable in vitro biocompatibility (Fig. 5A and B). Contrastively, MTX inhibited the proliferation of RAW264.7 and FLS when its concentration exceeded 200 μg/mL, implying the certain cytotoxicity of MTX (Fig. 5C and D). The stability of in vitro biocompatibility of MCDs was also investigated. When dissolved in DMEM medium and stored for 1 and 3 months, MCDs did not exhibit cytotoxicity on these two cells, indicating the stable and reliable biocompatibility (Fig. S15). Combined with the EC50 result of ABTS radical scavenging assay, the low (10 μg/mL), medium (30 μg/mL), and high (60 μg/mL) concentrations of MCDs were selected for evaluating the effects of MCDs on cells.

The intracellular ROS scavenging capability of MCDs was evaluated using the DCFH-DA probe to quantify oxidative stress in cells. LPS + IFN-γ stimulated RAW264.7 (M1 phenotype macrophages) and FLS showed a significantly brighter DCFH-DA fluorescence compared to unstimulated macrophages and normal FLS (Fig. 5E and F). In comparison, increased MCDs significantly reduced the green fluorescence in RAW264.7 and FLS. The quantified average fluorescence intensities of DCFH-DA in the intervention of high concentration MCDs decreased to about 78.15 ± 2.26% and 71.87 ± 3.67% compared with that in the LPS + IFN-γ-stimulated RAW264.7 and FLS, respectively (Fig. 5G and H). In addition, the SOD and CAT activity in LPS + IFN-γ stimulated RAW264.7 and FLS were significantly lower than control group (normal cells), while MCDs increased the SOD and CAT activity in a concentration-dependent manner (Fig. 5I-L). Meanwhile, the intracellular ROS scavenging performance of MCDs in THP-1-M and RA-FLS (Human-derived FLSs) were investigated and compared. Consistent with the results of RAW264.7 and FLS, MCDs could reduce the DCFH-DA fluorescence in LPS + IFN-γ-stimulated THP-1-M and RA-FLS (Fig. S16). The average fluorescence intensities with the treatment of 60 μg/mL MCDs decreased to about 66.37 ± 3.54% and 62.76 ± 4.83% compared with that in the LPS + IFN-γ-stimulated THP-1-M and RA-FLS, respectively (Fig. S17). Equally, the enhanced SOD and CAT activity in LPS + IFN-γ stimulated THP-1-M and RA-FLS could also be observed with

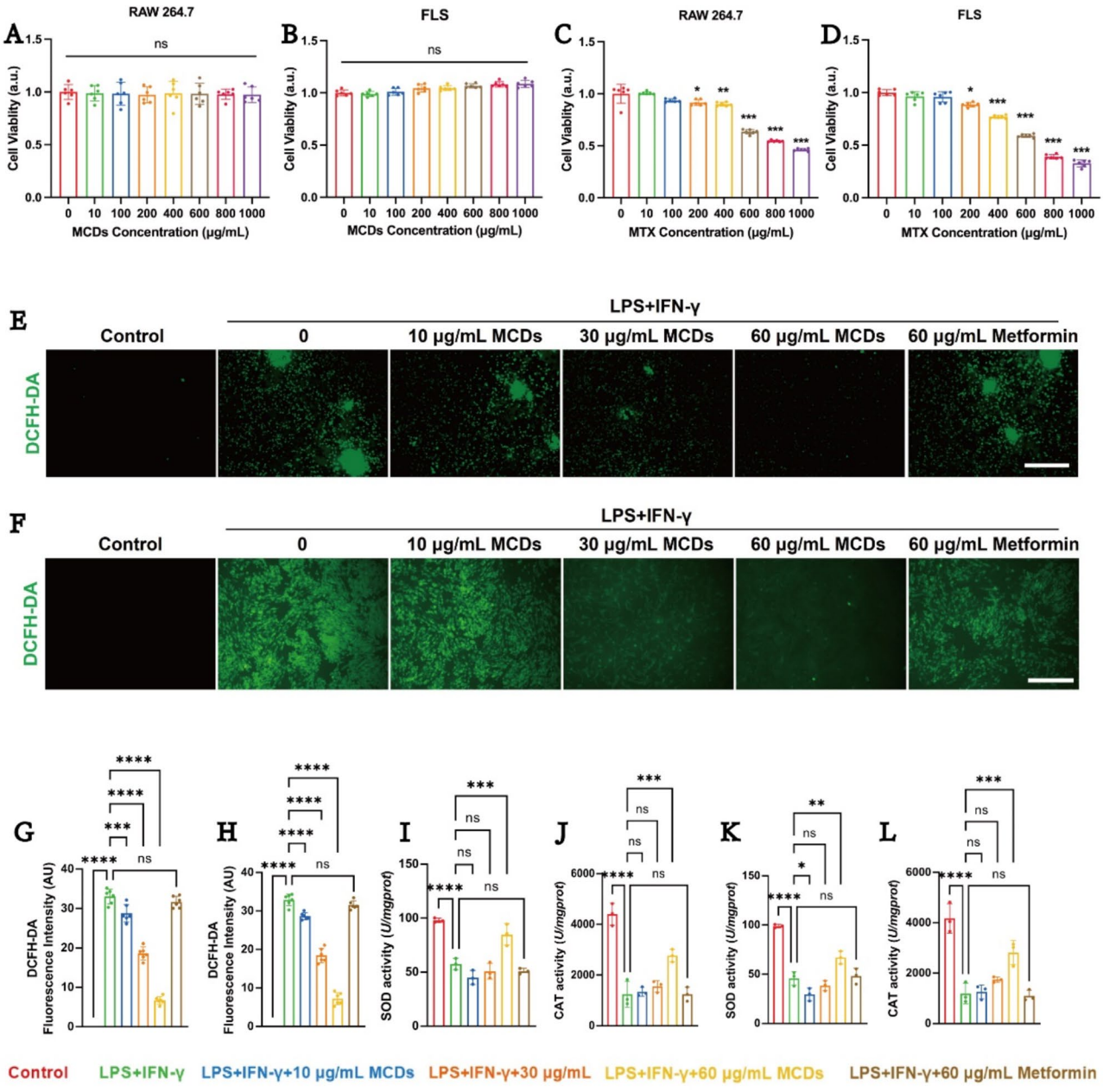

Fig. 5 In vitro antioxidant ability of MCDs. (**A**, **B**) Cell viability of RAW264.7 and FLS cultured with different concentrations of MCDs (0–1000 μg/mL) for 24 h. The values reported are mean ± SD, $n = 6$. (**C**, **D**) Cell viability of RAW264.7 and FLS cultured with different concentrations of MTX (0–1000 μg/mL) for 24 h. The values reported are mean ± SD, $n = 6$, $^{*}P < 0.05$, $^{**}P < 0.01$, $^{***}P < 0.001$. (**E**, **F**) Representative images of DCFH-DA staining in RAW264.7 and FLS after different intervention (Scar bar = 200 μm). (**G**, **H**) Quantitative results of DCFH-DA fluorescence intensity in RAW264.7 and FLS from different groups. The values reported are mean ± SD, $n = 6$, $^{*}P < 0.05$, $^{**}P < 0.01$, $^{***}P < 0.001$, $^{****}P < 0.0001$. (**I**, **J**) The SOD and CAT activity of RAW264.7 in different groups. The values reported are mean ± SD, $n = 3$, $^{*}P < 0.05$, $^{**}P < 0.01$, $^{***}P < 0.001$, $^{****}P < 0.0001$. (**K**, **L**) The SOD and CAT activity of FLS in different groups. The values reported are mean ± SD, $n = 3$, $^{*}P < 0.05$, $^{**}P < 0.01$, $^{***}P < 0.001$, $^{****}P < 0.0001$

the increased MCDs (Fig. S18). As the raw materials of MCDs, the intracellular antioxidant ability of metformin was also investigated. For DCFH-DA staining, metformin group showed no significant difference in average fluorescence intensities compared to that of LPS + IFN-γ stimulation (Fig. 5E-H, Fig. S16, Fig. S17). As for SOD and CAT activity, metformin could not significantly increase the intracellular SOD and CAT activity (Fig. 5I-L, Fig. S18). Above results highlight that there is a high level of oxidative stress in LPS + IFN-γ stimulated macrophages and FLSs, while MCDs can elevate the intracellular SOD and CAT activity to scavenging ROS, suggesting that MCDs are promising candidate to relieve oxidative stress for clinical RA therapy.

Since MCDs efficiently inhibit released pro-inflammatory cytokines in vivo, the role of MCDs in M1/M2 polarization was explored using mouse and human macrophage cell lines RAW264.7 and THP-1-M. The expression levels of M1 (TNF-α, IL-6) and M2 (IL-4, IL-10) markers in macrophage supernatant were studied and compared in unstimulated macrophages intervened with different concentrations of MCDs. After co-cultured with MCDs for 24 h, the expression level of M1 markers (TNF-α, IL-6) downregulated with the enhanced MCDs, with the significant difference with the control group in the 60 μg/mL MCDs group (Fig. 6A, Fig. S19A, S19B).

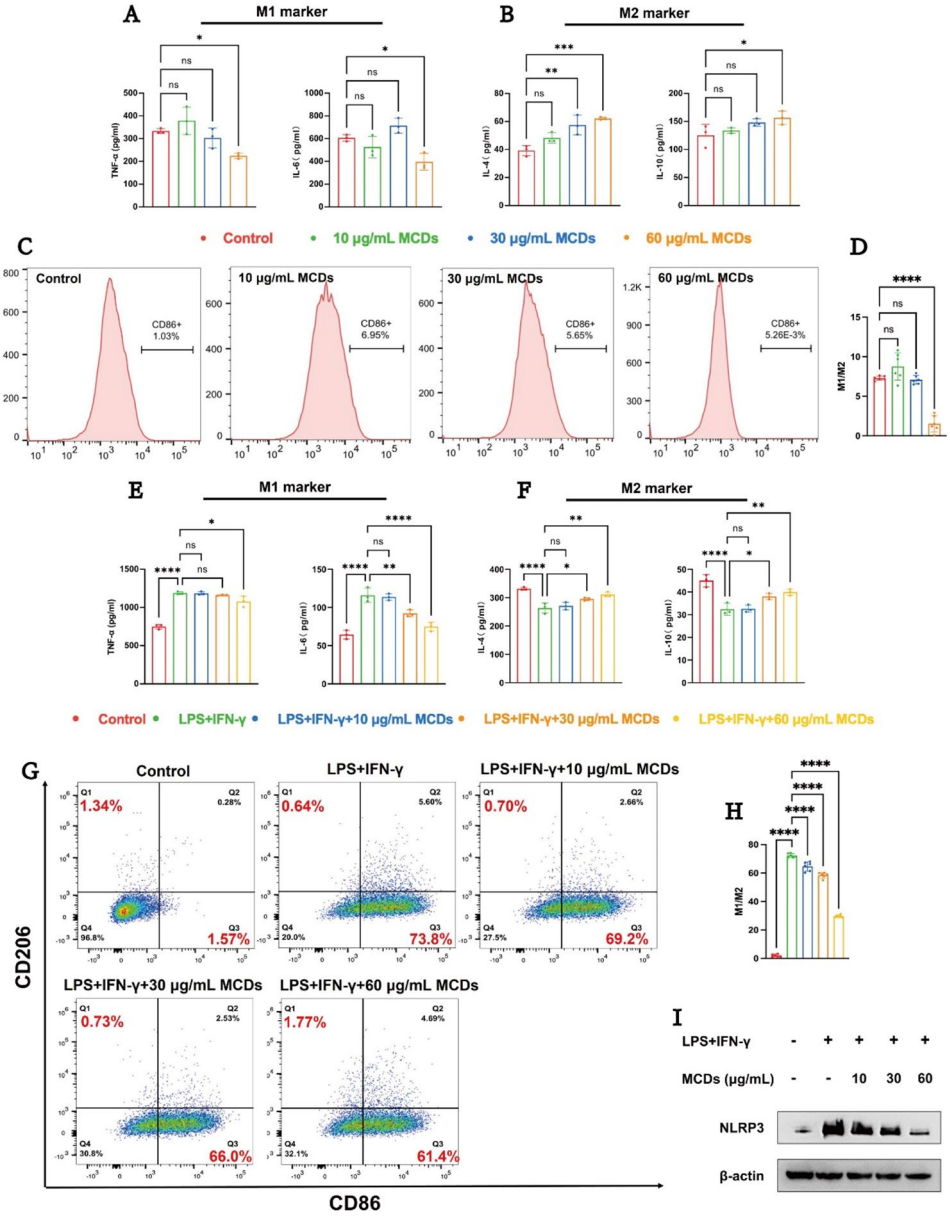

Fig. 6 MCDs induced macrophages polarization from pro-inflammatory M1 phenotype to anti-inflammatory M2 phenotype in normal and inflamed condition. (**A**, **B**) The expression level of M1 marker (TNF-α, IL-6) and M2 marker (IL-4, IL-10) in RAW264.7 cultured with different concentrations of MCDs without inflammation stimulation. The values reported are mean ± SD, $n = 3$, $^{*}P < 0.05$, $^{**}P < 0.01$, $^{***}P < 0.001$. (**C**) The M1 phenotype macrophage (CD86+) proportion of different groups in RAW264.7 without inflammation stimulation detected by flow cytometry. (**D**) Quantitative results of M1/M2 ratio from (**C**). The values reported are mean ± SD, $n = 6$, $^{*}P < 0.05$, $^{**}P < 0.01$, $^{***}P < 0.001$, $^{****}P < 0.0001$. (**E**, **F**) The expression level of M1 marker (TNF-α, IL-6) and M2 marker (IL-4, IL-10) in RAW264.7 cultured with different concentrations of MCDs with LPS + IFN-γ stimulation. The values reported are mean ± SD, $n = 3$, $^{*}P < 0.05$, $^{**}P < 0.01$, $^{***}P < 0.001$, $^{****}P < 0.0001$. (**G**) The M1 phenotype (CD86+) and M2 phenotype (CD206+) macrophage proportion of different groups in RAW264.7 with LPS + IFN-γ stimulation detected by flow cytometry. (**H**) Quantitative results of M1/M2 ratio from (**G**). The values reported are mean ± SD, $n = 6$, $^{*}P < 0.05$, $^{**}P < 0.01$, $^{***}P < 0.001$, $^{****}P < 0.0001$. (**I**) The protein expression level of NLRP3 in RAW264.7 after different intervention detected by western blot

Correspondingly, the M2 markers (IL-4, IL-10) expression level upregulated with the increased concentration of MCDs. Among them, the 10 μg/mL MCDs and 30 μg/mL MCDs groups showed no significant difference with the control group, while the 60 μg/mL MCDs group increased distinctly (Fig. 6B, Fig. S19C, S19D). Moreover, macrophage polarization in RAW264.7 and THP-1-M was evaluated by flow cytometry after staining with anti-CD86 (M1 biomarker) and anti-CD206 (M2 biomarker). Consistent with the ELISA results, the M1/M2 ratios decreased from 7.16 ± 1.14 and 5.92 ± 1.09 to 2.27 ± 0.87 and 1.87 ± 0.23 in RAW264.7 and THP-1-M, respectively (Fig. 6C and D, Fig. S20).

When pretreated by LPS + IFN-γ, the expression level of M1 markers (TNF-α, IL-6) increased substantially compared to the control group, while M2 markers (IL-4, IL-10) were suppressed under inflammation (Fig. 6E and F, Fig. S21). While, MCDs treatment can effectively reversed these situations, normalizing the expression levels of both M1 and M2 markers. Stimulated by LPS + IFN-γ, the proportion of M1 macrophages was greatly increased to 73.8% and 13.7% compared to the control group in RAW264.7 and THP-1-M, respectively (Fig. 6G and H, Fig. S22). Nevertheless, MCDs treatment reduced the proportion of M1 macrophages to 61.4% and 0.094%, while the proportion of M2 macrophages increased from 0.64% and 3.32–1.77% and 21.6% in RAW264.7 and THP-1-M, respectively. These results suggest that the anti-inflammatory effect of MCDs contributes largely to the transformation of macrophages from M1 to M2 phenotype in normal and inflammatory conditions. The immunoregulation stability of MCDs was further investigated. After 1 and 3 months of storage, MCDs still could downregulate the expression level of M1 markers (TNF-α, IL-6) while upregulate the M2 markers (IL-4, IL-10) expression, particularly at higher concentrations of MCDs (Fig. S23).

The activation of NLRP3 inflammasome, which can be induced by oxidative stress, promotes structural changes in NLRP3 and enhances its formation in M1 macrophages, leading to increased M1 polarization [65]. Taking into account the proved antioxidant performance and promoting M2 macrophages polarization of MCDs, the association of macrophages polarization and the inhibition of the NLRP3 inflammasome caused by MCDs were explored in RA model using western blot. In the presence of LPS + IFN-γ, the protein expression level of NLRP3 was greatly increased via stimulation compared to unstimulated RAW264.7 and THP-1-M (control group) (Fig. 6I, Fig. S24, Fig. S25). MCDs treatment resulted in a marked reduction in NLRP3 expression. Moreover, treated cells with high concentration of MCDs showed no significant difference with the control groups (Fig. 6I, Fig. S24, Fig. S25). The results support that MCDs possibly realize macrophage M2 type polarization through inhibiting NLRP3 inflammasome signaling pathway, which is activated under oxidative stress and pro-inflammatory conditions in RA.

MCDs inhibit synovium inflammation and fibrosis by blocking IL-6/gp130 signaling pathway

Besides macrophages, the severity and progression of RA is also influenced by FLSs [66]. As the confirmed in vivo potency of MCDs by reducing the inflammation and fibrosis level, the in vitro effects of MCDs on the proliferation, migration, apoptosis, and fibrosis of FLSs were studied to understand their underlying mechanisms. The FLS and RA-FLS were applied as the representative model cells. Compared to the control group, the cell viabilities of FLS and RA-FLS significantly increased with LPS + IFN-γ stimulation (Fig. 7A, Fig. S26), suggesting that the hyperplasia of FLS and RA-FLS occurred in inflammatory environment. However, the hyperplasia began to decrease as the added MCDs, and gradually reduced to normal levels with 60 μg/mL MCDs treatment.

The effect of MCDs on FLSs apoptosis under inflammatory condition was evaluated by flow cytometry. As shown in Fig. 7B and C and Fig. S27, the rate of apoptosis in LPS + IFN-γ stimulated two cell types were significantly lower than the control group, indicating that FLSs underwent less apoptosis in the inflammatory environment, which was consistent with the results of its excessive proliferation. After incubation with MCDs, the rate of apoptosis increased from 0.10 ± 0.04% and 5.26 ± 1.07% to 21.39 ± 2.51% and 38.69 ± 2.74% in FLS and RA-FLS, respectively. These results indicate that MCDs significantly promote synoviocyte apoptosis under inflammatory conditions.

Then, the migration of FLSs was studied by Transwell assay. In normal conditions, there was no significant difference in the number of migration cells between the MCDs-treated groups and the control group, indicating that MCDs had minimal effect on FLSs migration under these conditions (Fig. S28, Fig. S29). However, the migration of LPS + IFN-γ-stimulated FLSs remarkably increased compared to the control group (Fig. 7D and E, Fig. S30). Meanwhile, the migration cell number of FLSs gradually decreased in a concentration-dependent manner with the intervention of MCDs in the inflammatory environment.

The potential inhibition of MCDs on the inflammation and fibrosis were evaluated by monitoring the intracellular expression level of TNF-α, IL-6, α-SMA, and Col-I in activated FLSs. Stimulated by LPS + IFN-γ, the expression levels of TNF-α, IL-6, α-SMA, and Col-I in FLSs were significantly increased compared to the control group, indicating a higher inflammation and fibrosis

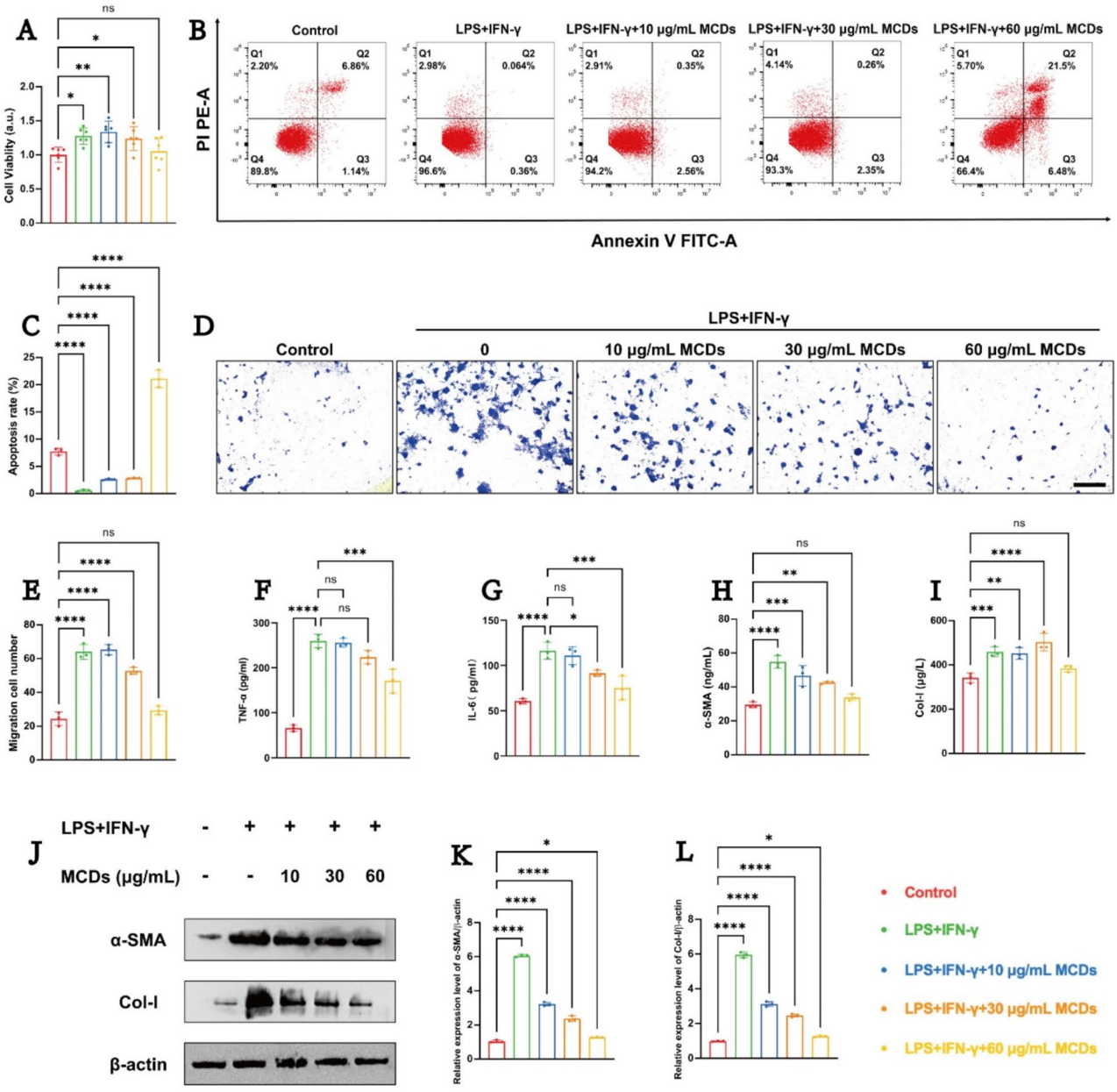

Fig. 7 MCDs inhibited the proliferation, migration, inflammation, and fibrosis in FLSs. (**A**) Cell viability of inflamed FLS exposed to different concentrations of MCDs for 24 h. The values reported are mean ± SD, $n = 6$, $^{*}P < 0.05$, $^{**}P < 0.01$, $^{***}P < 0.001$. (**B**) Flow cytometry assay to evaluate the impact of MCDs on inflamed FLS's apoptosis. (**C**) Quantitative results of apoptosis rate in different groups from (**B**). The values reported are mean ± SD, $n = 3$, $^{*}P < 0.05$, $^{**}P < 0.01$, $^{***}P < 0.001$, $^{****}P < 0.0001$. (**D**) Representative images of inflamed FLS's migration under different intervention by Transwell assay (Scar bar = 200 μm). (**E**) Quantitative results of migration cell number in different groups from (**D**). The values reported are mean ± SD, $n = 3$, $^{*}P < 0.05$, $^{**}P < 0.01$, $^{***}P < 0.001$, $^{****}P < 0.0001$. (**F-I**) The expression level of TNF-α, IL-6, α-SMA, and Col-I in inflamed FLS with MCDs treatment. The values reported are mean ± SD, $n = 3$, $^{*}P < 0.05$, $^{**}P < 0.01$, $^{***}P < 0.001$, $^{****}P < 0.0001$. (**J**) Protein band results of α-SMA and Col-I in inflamed FLS after different intervention. (**K**, **L**) Quantitative results of α-SMA and Col-I protein expression level in different groups from (**J**). The values reported are mean ± SD, $n = 3$, $^{*}P < 0.05$, $^{**}P < 0.01$, $^{***}P < 0.001$, $^{****}P < 0.0001$

existed in mimetic RA microenvironment (Fig. 7F-I, Fig. S31). When treated with MCDs, the relative expression level of TNF-α, IL-6, α-SMA, and Col-I gradually decreased. Consist with the ELISA results, the western blot (Fig. 7J-L, Fig. S32) implied that the expression level of the fibrosis indicators (α-SMA and Col-I) generally downregulated with the intervention of MCDs. Considering macrophages and FLSs are the main cells involved in RA, the interaction between the two cells were clarified using a co-culture model of macrophages and FLSs through Transwell plates (Fig. 8A). Equally, the intracellular expression levels of inflammation (TNF-α, IL-6) and

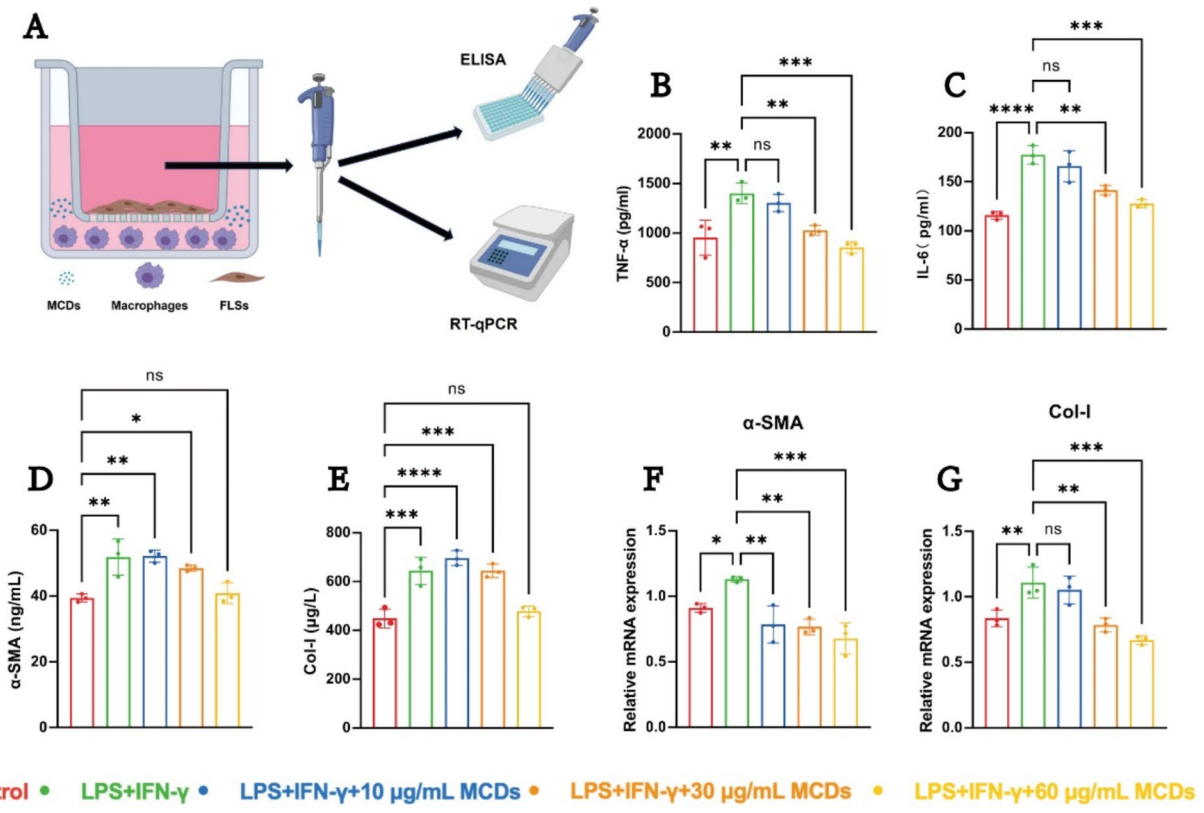

Fig. 8 MCDs exerted anti-inflammatory and anti-fibrosis effect in FLSs through macrophage immunoregulation by Transwell co-culture. (**A**) The schematic illustration of the co-cultured model of FLSs and macrophages. (**B**-**E**) The expression level of TNF-α, IL-6, α-SMA, and Col-I in inflamed FLS after different concentrations of MCDs cultured with RAW264.7. The values reported are mean ± SD, $n = 3$, $^{*}P < 0.05$, $^{**}P < 0.01$, $^{***}P < 0.001$, $^{****}P < 0.0001$. (**F**, **G**) The mRNA expression level of α-SMA and Col-I in inflamed FLS after different concentrations of MCDs cultured with RAW264.7. The values reported are mean ± SD, $n = 3$, $^{*}P < 0.05$, $^{**}P < 0.01$, $^{***}P < 0.001$

fibrosis (α-SMA, Col-I) in different groups were detected by ELISA. The expression levels of TNF-α, IL-6, α-SMA, and Col-I in FLSs were significantly higher than those in the control group (Fig. 8B-E, Fig. S33). The expression levels of TNF-α, IL-6, α-SMA, and Col-I in the FLSs showed a corresponding downward trend with the treatment of the co-culture of MCDs and macrophages. Furthermore, compared to the LPS + IFN-γ stimulated group, the mRNA expression levels of α-SMA and Col-I in FLSs decreased with the intervention of MCDs (Fig. 8F and G, Fig. S34), consistent with the results of ELISA assay. All these findings indicate that MCDs not only directly reduce the intracellular expression level of inflammation and fibrosis in FLSs, but also suppress relative expression of inflammation and fibrosis through the immunoregulation of macrophages. At the same time, the efficacy of MCDs in maintaining homeostasis of FLSs under inflammatory environment has also been validated in human-derived FLSs, indicating its potential application in clinical antirheumatic therapy.

The modulation of IL-6/gp130 pathway can affect the synovial inflammation and the proliferation, migration and fibrosis of FLSs at the same time [27]. Figure 6 confirms that MCDs induce the polarization of macrophages from M1 phenotype to M2 phenotype with the reduced secretion of IL-6. In addition, MCDs exerts immunomodulatory effects on macrophages and reduces the expression level of IL-6 and fibrosis related indicators in FLSs based on co-culture Transwell model (Fig. 8). IL-6 is the upstream of gp130 [67]. It is hypothesized that MCDs inhibit the proliferation, migration and fibrosis of FLSs by inhibiting the IL-6/gp130 pathway, while reducing the level of intracellular inflammation. The co-culture model of macrophages and FLSs (Fig. 8A) was further used to evaluate the effects of MCDs on the protein expression levels of IL-6 and gp130 in inflammatory environment by western blot. It was found that the protein expression levels of IL-6 and gp130 in FLSs were significantly increased after macrophages stimulated by LPS + IFN-γ (Fig. 9A-C, Fig. S35). The protein expression levels of IL-6 and gp130 in FLSs gradually decreased after the intervention of the enhanced MCDs. Besides, immunohistochemical analysis suggested that the synovium expression level of gp130 reduced as the increased does of MCDs in CIA rats (Fig. S36). Furthermore, the effects of MCDs on proliferation, migration and fibrosis of FLSs

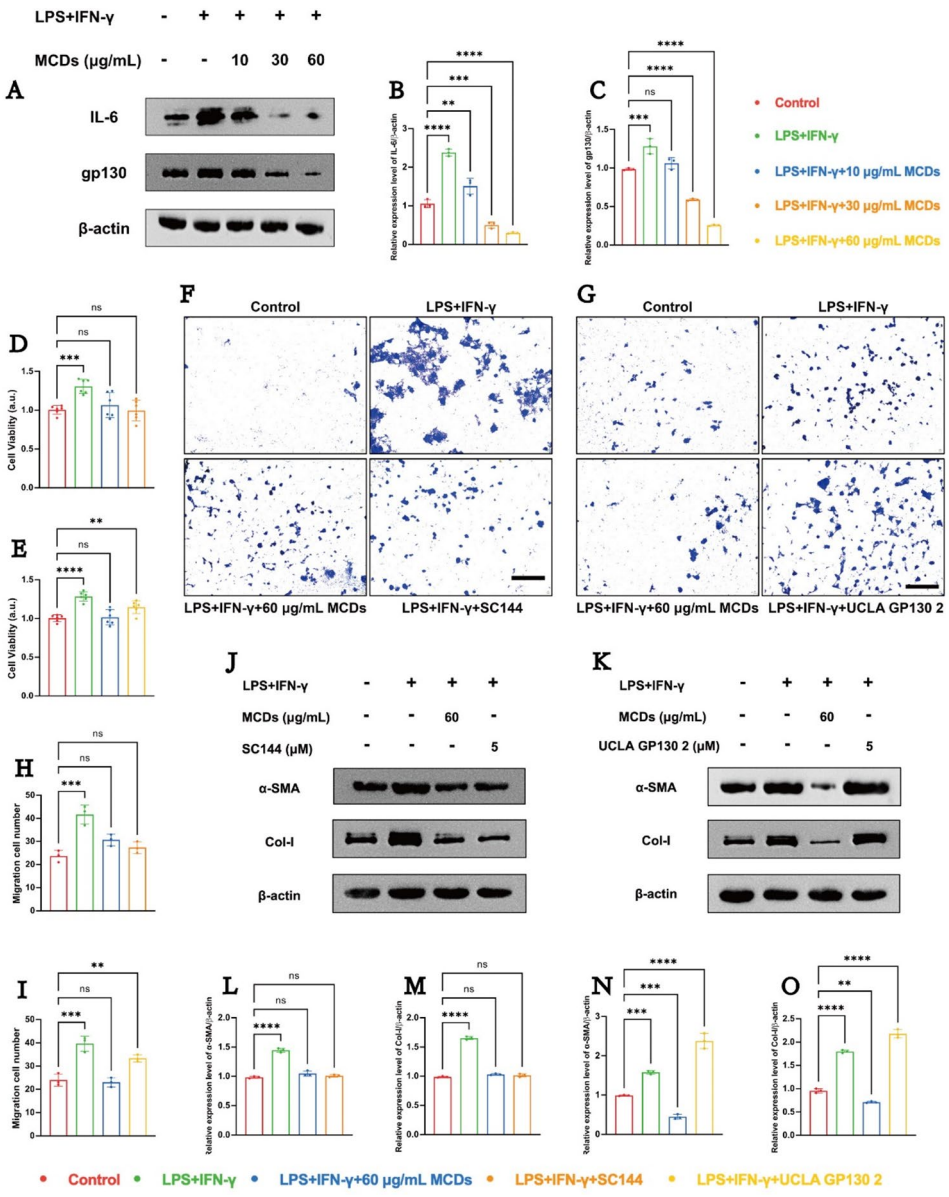

Fig. 9 MCDs achieve anti-inflammation and suppress the proliferation, migration and fibrosis of FLSs by inhibiting IL-6/gp130 signaling pathway. (**A**) Protein band results of IL-6 and gp130 in inflamed FLS after different intervention. (**B**, **C**) Quantitative results of IL-6 and gp130 protein expression level in inflamed FLS from (**A**). The values reported are mean ± SD, $n = 3$, $^{*}P < 0.05$, $^{**}P < 0.01$, $^{***}P < 0.001$, $^{****}P < 0.0001$. (**D**, **E**) Cell viability of inflamed FLS exposed to MCDs, gp130 inhibitor (SC144), gp130 activator (UCLA GP130 2) for 24 h. The values reported are mean ± SD, $n = 6$, $^{*}P < 0.05$, $^{**}P < 0.01$, $^{***}P < 0.001$, $^{****}P < 0.0001$. (**F**, **G**) Representative images of inflamed FLS's migration under different intervention by Transwell assay (Scar bar = 200 μm). (**H**, **I**) Quantitative results of migration cell number in different groups from (**F**, **G**). The values reported are mean ± SD, $n = 3$, $^{*}P < 0.05$, $^{**}P < 0.01$, $^{***}P < 0.001$. (**J**, **K**) Protein band results of α-SMA and Col-I in inflamed FLS after different intervention. (**L**-**O**) Quantitative results of α-SMA and Col-I protein expression level in inflamed FLS from (**J**, **K**). The values reported are mean ± SD, $n = 3$, $^{*}P < 0.05$, $^{**}P < 0.01$, $^{***}P < 0.001$, $^{****}P < 0.0001$

after intervention of gp130 were evaluated by introducing gp130 inhibitor (SC144) and activator (UCLA GP130 2). As for proliferation, the cell viability of FLSs decreased significantly after the intervention of MCDs and SC144 compared to the inflammation modeling group, and showed similar cell viability to the control group (Fig. 9D and E, Fig. S37). Correspondingly, the proliferation activity of FLSs significantly increased compared to the normal cells after UCLA GP130 2 treatments. By Transwell assay, the number of cell migration in FLSs began to decline similar to that in MCDs with adding SC144, and showed no significant difference with the normal cells (Fig. 9F and H, Fig. S38). On the other hand, UCLA GP130 2 treatments significantly increased FLSs migration compared to the control group and MCDs-treated group (Fig. 9G and I, Fig. S39). Correspondingly, the

fibrosis related indexes (α-SMA, Col-I) decreased similar to that of the MCDs and control group with treating SC144 (Fig. 9J, L and M, Fig. S40). Nevertheless, the protein expression levels of α-SMA and Col-I in FLSs increased significantly compared to the MCDs and control group following the UCLA GP130 2 interventions (Fig. 9K, N and O, Fig. S41). Therefore, gp130 activator could promote the proliferation, migration and fibrosis of FLSs in inflammatory condition, while both gp130 inhibitor and MCDs is able to suppress the above activities. To sum up, MCDs achieve anti-inflammation and suppress the proliferation, migration and fibrosis of FLSs by inhibiting IL-6/gp130 signaling pathway.

Discussion

Nowadays, RA presents a significant challenge to clinicians and researchers due to its complex and not fully understood etiology and pathogenesis. Redox imbalance and chronic inflammation are the two major features of RA. Excessive production of ROS could trigger the release of pro-inflammatory cytokines from immune cells, aggravating the inflammatory response. This heightened inflammation, in turn, increases oxidative stress, creating a vicious cycle of injury and inflammation [68, 69]. In addition, persistent synovial inflammation can lead to bone erosion and excessive proliferation and invasion of FLSs, ultimately resulting in joint dysfunction in RA patients [66, 70]. Current antirheumatic drugs can partially alleviate the symptoms of RA, but they are associated with a series of long-term side effects [29, 66]. These drugs typically suffer from low specificity and undergo rapid metabolism and clearance from the body [71]. Nanomaterials and nanomedicine offer promising directions for the treatment of RA [64, 72]. Nanodrug delivery systems have been implemented to address RA by improving drug stability, controlled release, and targeted delivery [72, 73]. Despite these advancements, existing nanomaterials often fail to fully address the specific microenvironment of RA and lack a thorough understanding of their underlying mechanisms.

Ideal medications or biomaterials for treating RA should effectively target both the inflamed joints and the relevant inflamed cells. As a first-line treatment for RA, MTX is effective in controlling disease progression and serves as a representative therapy in this regard. The use of MTX and other medications still have the problem of off-target [74, 75]. Due to the lack of the modification of antibodies or ligand on MCDs, it is hard for MCDs achieving specific active targeting based on certain molecular mechanism [76]. Specific particle size of nanomaterials could passively target inflamed sites due to ELVIS effect. MCDs can achieve passive targeting and accumulation through the physicochemical properties. The characterization of MCDs showed the average size of 3.1 nm and spherical structure. The targetability of MCDs to RA was found in vitro and in vivo. The cell uptake assay showed that MCDs could be uptaken by RAW264.7 and FLS in normal condition, while it appeared more enrichment by inflammatory FLS. The in vivo biodistribution results showed that MCDs could accumulated in inflamed joints of CIA rats. Optimal biocompatibility is also of importance for clinical application. Long-term administration of MTX commonly results in systemic toxicity [77, 78]. Impaired liver and kidney function were observed in CIA rats after two weeks of intravenous injection of MTX according to histopathological and blood biochemical tests. Invisible cytotoxicity was found in macrophages and FLSs when MTX's concentration exceeded 400 μg/mL. Carbon dots are widely used in the biomedical field because of the favorable biocompatibility [79]. To realize this vision, the synthetic and preparation of MCDs aims to address RA through systemic administration. Indeed, little damages were observed in the structure and function of main organs in CIA rat with the treating period of MCDs. Simultaneously, MCDs behaved excellent biocompatibility when cultured with macrophages and FLSs. Above results demonstrated that MCDs owned preferable targetability in inflamed cells and joints as well as favorable biocompatibility compared to MTX, which laid a robust foundation for the management of RA.

There is a high level of synovial inflammation and overproduction of ROS at inflamed sites in RA. Researchers focus on developing strategies that serve as an antioxidant while also inducing macrophages polarization to exert an anti-inflammatory effect [80, 81]. Our previous work has indicated that antioxidant CDs exhibited well performance in scavenging relative free radicals [44]. The molecular structure of the MCDs included amido, hydroxide, and carboxyl groups, which are significant for their antioxidant function. Similarly, MCDs realized favorable radical scavenging activity to ABTS, $O_2^{\bullet-}$, and H_2O_2. In CIA rats or inflamed macrophages/FLSs, MCDs elevated the SOD and CAT activity to scavenging $O_2^{\bullet-}$ and H_2O_2 for the achievement of preferable antioxidant performance. Besides, MCDs could increase the expression of anti-inflammatory cytokines (IL-4, IL-10) while reduce the pro-inflammatory cytokines (TNF-α, IL-6) expression in CIA rats. Accordingly, the level of synovial inflammation in CIA rats decreased, and the progression of bone erosion also prohibited. MCDs could downregulated the expression level of M1 biomarker (TNF-α, IL-6), while upregulated the M2 biomarker (IL-4, IL-10) expression level whether in normal or LPS + IFN-γ stimulated macrophages. Notably, NLRP3 inflammasome is closely associated with immunoregulation. Activated NLRP3 inflammasome could induce M1 phenotype macrophage with the released pro-inflammatory cytokines.

In this study, MCDs downregulated the expression level of NLRP3 in inflamed macrophages as well as effectively scavenging overproduction of intracellular ROS. In depth, MCDs exerted immunoregulation effect through inhibiting NLRP3 inflammasome signaling pathway. MCDs possessed satisfied antioxidant ability, and induced macrophages polarization from M1 phenotype to M2 phenotype to realizing anti-inflammatory effect.

Nevertheless, antioxidant and anti-inflammatory therapy cannot achieve fully remission for RA [82]. Overproliferation, invasion, and fibrosis of FLSs gradually become the focus of research which is considered as the promising therapeutic target for RA [83, 84]. The severe synovial hyperplasia and fibrosis of FLSs were found in CIA rats compared to the normal rats through histology and immunohistochemistry. After the intravenous treatment of MCDs, prohibited synovial hyperplasia and downregulated expression level of fibrosis related indicators (α-SMA, Col-I) were observed. Equally, more visible cell proliferation, less apoptosis, remarkable migration, and upregulated expression level of fibrosis were discovered in LPS + IFN-γ stimulated FLSs. MCDs reduced the cell viability and promoted the apoptosis rate of inflamed FLSs. The results of Transwell assay suggested that MCDs exhibited no effect on the migration of FLSs while inhibited the migration under inflammation condition. Besides, MCDs could reduce the expression level of inflammation and fibrosis in inflammatory FLSs. The co-culture model further confirmed that MCDs downregulated the expression of inflammatory and fibrosis indicators in FLSs through interacting with macrophages. Importantly, the similar therapeutic effects of MCDs on mouse-derived FLSs could be achieved in human-derived FLSs, indicating the great clinical application prospect of MCDs in antirheumatic therapy. Furthermore, the molecular mechanism by which MCDs exerted the effects on FLSs indicated that MCDs could downregulate the expression level of IL-6 and gp130 (the downstream of IL-6). The relative results by introducing the inhibitor and activator of gp130 implied that MCDs acted as a gp130 inhibitor. Hence, MCDs exerted anti-inflammatory effects while suppressing the proliferation, migration, and fibrosis of FLSs by blocking the IL-6/gp130 signaling pathway.

In brief, the CIA animal and inflamed cell models were constructed and applied to evaluate the treating effect of MCDs on RA in vivo and in vitro with the clarified mechanism. Though favorable therapeutic effect observed, there are still some limitations in this study. First, bone erosion is a significant symptom of severe RA. Although MCDs show visibly superior bone repair effect similar to MTX, there are lack of more evidences for the detailed inhibition process of MCDs on bone erosion and destruction in vitro. Next, macrophages (RAW264.7, THP-1-M) and FLSs (FLS, RA-FLS) are adopted in this study, and stimulated by LPS + IFN-γ to mimic in vitro model of RA. However, these cell lines do not fully represent the real disease microenvironment of RA. It would be preferable to select macrophages and FLSs isolated from RA animal model or patients for further study. Then, as an autoimmune disease, the pathogenesis of RA is relatively complex. Despite of adaptive immunity, innate immunity also participates in the progression of RA [85, 86]. Since pro-inflammatory cytokines have been reported to activate various innate immune cells, including natural killer cells, mast cells, dendritic cells and so on [87–89]. It is possible that MCDs may exert antirheumatic effects by regulating innate immune cells. Also, a dynamic observation and comparison lacked in the animal study. For example, more observation time points which used for radiology and histopathological analysis were more appropriate for therapeutic evaluation. In addition, biochemical analysis before treatment should be served as baseline data for comparing post-treatment indicators, which would be better for monitoring therapeutic effect and safety of MCDs during therapy period. Finally, it is concluded that MCDs realize the immunoregulation of macrophages and homeostasis of FLSs through regulating the expression of NLRP3, IL-6, and gp130. Nevertheless, further exploration is needed to elucidate the precise regulatory mechanisms of MCDs and their corresponding molecular pathways.

Conclusion

To address RA through the modulation of the disease microenvironment, metformin-derived CDs (MCDs) were synthesized using one-step hydrothermal method. MCDs demonstrated effective accumulation in the inflamed joints and inhibited the progression of arthritis, inflammation infiltration, synovial hyperplasia, bone erosion, and synovial fibrosis in RA animal models. Furthermore, MCDs not only promoted the polarization of macrophages towards M2 phenotype without stimulation, but also eliminated the cellular ROS in RA microenvironment as well as inhibiting NLRP3 inflammasome signaling pathway, effectively polarized them into the M2 phenotype to realize the anti-inflammatory effect. Meanwhile, MCDs inhibited the proliferation, migration, and fibrosis in FLSs while reducing the level of synovial inflammation by blocking IL-6/gp130 signaling pathway. In vivo and in vitro results collectively demonstrated that MCDs could reshape the inflammatory RA microenvironment into anti-inflammatory state by scavenging overproduction of ROS, promoting the M1 phenotype to M2 phenotype macrophage repolarization, and restoring the homeostasis of FLSs. Taken together, the designed MCDs with prominent biocompatibility, antioxidant, and

anti-inflammatory activities provides a promising therapeutic strategy for RA.

Supplementary Information

The online version contains supplementary material available at https://doi.org/10.1186/s12951-025-03159-7.

Supplementary Material 1

Acknowledgements
The authors thank Mr. Junjin Lin from the Public Technology Service Center Fujian Medical University for the technical guidance and assistance on flow cytometry and CLSM imaging in this work.

Author contributions
Rui Zhang: Conceptualization, Data curation, Formal analysis, Investigation, Writing – original draft. Xingyu Lin: Data curation, Formal analysis, Investigation, Methodology. Rongjie Lin: Formal analysis, Investigation, Methodology, Software. Zhenbin Chen: Investigation, Methodology, Software. Chenfang Miao: Formal analysis, Investigation, SoftwareYao Wang: Resources, Software, Xiaoqin Deng: Formal analysis. Jianlong Lin: Data curation. Shishui Lin: Investigation, Project administration, Supervision. Shaohuang Weng: Conceptualization, Funding acquisition, Project administration, Supervision, Writing – original draft, Writing –review & editing. Min Chen: Funding acquisition Project administration, Supervision, Writing – original draft, Writing – review & editing. All authors reviewed the manuscript.

Funding
This work was finically supported by the Joint Funds for the Innovation of Science and Technology, Fujian Province (Nos. 2021Y9081, 2021Y9007).

Data availability
No datasets were generated or analysed during the current study.

Declarations

Ethics approval and consent to participate
Ethical approval for the in vivo experiments was granted by the Institutional Animal Care and Use Committee of Fujian Medical University (IACUC FJMU 2023 – 0149).

Consent for publication
Not applicable.

Competing interests
The authors declare no competing interests.

Author details
[1]Department of Orthopedic Surgery, Fujian Medical University Union Hospital, Fuzhou 350001, China
[2]Department of Pharmaceutical Analysis, School of Pharmacy, Fujian Medical University, Fuzhou 350122, China
[3]Department of Orthopedic Surgery, Shengli Clinical Medical College of Fujian Medical University, Fuzhou University Affiliated Provincial Hospital, Fuzhou 350001, China

Received: 17 September 2024 / Accepted: 22 January 2025
Published online: 29 January 2025

References

1. Lai B, Wu CH, Lai JH. Activation of c-Jun N-Terminal kinase, a potential therapeutic target in Autoimmune Arthritis. Cells. 2020;9(11):2466. https://doi.org/10.3390/cells9112466.
2. Smolen JS, Aletaha D, Barton A, Burmester GR, Emery P, Firestein GS, Kavanaugh A, McInnes IB, Solomon DH, Strand V, Yamamoto K. Rheumatoid arthritis. Nat Rev Dis Primers. 2018;4:18001. https://doi.org/10.1038/nrdp.2018.1.
3. Di Matteo A, Bathon JM, Emery P. Rheumatoid arthritis. Lancet. 2023;402(10416):2019–33. https://doi.org/10.1016/s0140-6736(23)01525-8.
4. Gravallese EM, Firestein GS. Rheumatoid arthritis - common origins, divergent mechanisms. N Engl J Med. 2023;388(6):529–42. https://doi.org/10.1056/NEJMra2103726.
5. Schönenberger KA, Schüpfer AC, Gloy VL, Hasler P, Stanga Z, Kaegi-Braun N, Reber E. Effect of anti-inflammatory diets on Pain in Rheumatoid Arthritis: a systematic review and Meta-analysis. Nutrients. 2021;13(12):4221. https://doi.org/10.3390/nu13124221.
6. Zhao Z, Hua Z, Luo X, Li Y, Yu L, Li M, Lu C, Zhao T, Liu Y. Application and pharmacological mechanism of methotrexate in rheumatoid arthritis. Biomed Pharmacother. 2022;150:113074. https://doi.org/10.1016/j.biopha.2022.113074.
7. Hoisnard L, Pina Vegas L, Dray-Spira R, Weill A, Zureik M, Sbidian E. Risk of major adverse cardiovascular and venous thromboembolism events in patients with rheumatoid arthritis exposed to JAK inhibitors versus adalimumab: a nationwide cohort study. Ann Rheum Dis. 2023;82(2):182–8. https://doi.org/10.1136/ard-2022-222824.
8. Weyand CM, Goronzy JJ. Immunometabolism in the development of rheumatoid arthritis. Immunol Rev. 2020;294(1):177–87. https://doi.org/10.1111/imr.12838.
9. You DG, Lim GT, Kwon S, Um W, Oh BH, Song SH, Lee J, Jo DG, Cho YW, Park JH. Metabolically engineered stem cell-derived exosomes to regulate macrophage heterogeneity in rheumatoid arthritis. Sci Adv. 2021;7(23):eabe0083. https://doi.org/10.1126/sciadv.abe0083.
10. Di Benedetto P, Ruscitti P, Vadasz Z, Toubi E, Giacomelli R. Macrophages with regulatory functions, a possible new therapeutic perspective in autoimmune diseases. Autoimmun Rev. 2019;18(10):102369. https://doi.org/10.1016/j.autrev.2019.102369.
11. Davies LC, Jenkins SJ, Allen JE, Taylor PR. Tissue-resident macrophages. Nat Immunol. 2013;14(10):986–95. https://doi.org/10.1038/ni.2705.
12. Li M, Yin H, Yan Z, Li H, Wu J, Wang Y, Wei F, Tian G, Ning C, Li H, Gao C, Fu L, Jiang S, Chen M, Sui X, Liu S, Chen Z, Guo Q. The immune microenvironment in cartilage injury and repair. Acta Biomater. 2022;140:23–42. https://doi.org/10.1016/j.actbio.2021.12.006.
13. Sadri B, Hassanzadeh M, Bagherifard A, Mohammadi J, Alikhani M, Moeinabadi-Bidgoli K, Madani H, Diaz-Solano D, Karimi S, Mehrazmay M, Mohammadpour M, Vosough M. Cartilage regeneration and inflammation modulation in knee osteoarthritis following injection of allogeneic adipose-derived mesenchymal stromal cells: a phase II, triple-blinded, placebo controlled, randomized trial. Stem Cell Res Ther. 2023;14(1):162. https://doi.org/10.1186/s13287-023-03359-8.
14. Chávez MD, Tse HM. Targeting mitochondrial-derived reactive oxygen species in T cell-mediated Autoimmune diseases. Front Immunol. 2021;12:703972. https://doi.org/10.3389/fimmu.2021.703972.
15. Gao J, Zhang H, Yang Y, Tao J. Therapeutic potential of targeting the NLRP3 inflammasome in rheumatoid arthritis. Inflammation. 2023;46(3):835–52. https://doi.org/10.1007/s10753-023-01795-5.
16. Shi S, Chen Y, Luo Z, Nie G, Dai Y. Role of oxidative stress and inflammation-related signaling pathways in doxorubicin-induced cardiomyopathy. Cell Commun Signal. 2023;21(1):61. https://doi.org/10.1186/s12964-023-01077-5.
17. Wei S, Xiao Z, Huang J, Peng Z, Zhang B, Li W. Disulfiram inhibits oxidative stress and NLRP3 inflammasome activation to prevent LPS-induced cardiac injury. Int Immunopharmacol. 2022;105:108545. https://doi.org/10.1016/j.intimp.2022.108545.
18. Bao M, Wang K, Li J, Li Y, Zhu H, Lu M, Zhang Y, Fan Q, Han L, Wang K, Wang D, Gao Y, Peng B, Ming Z, Liu W. ROS scavenging and inflammation-directed polydopamine nanoparticles regulate gut immunity and flora therapy in inflammatory bowel disease. Acta Biomater. 2023;161:250–64. https://doi.org/10.1016/j.actbio.2023.02.026.
19. Tur J, Pereira-Lopes S, Vico T, Marín EA, Muñoz JP, Hernández-Alvarez M, Cardona PJ, Zorzano A, Lloberas J, Celada A. Mitofusin 2 in Macrophages Links mitochondrial ROS production, Cytokine Release, Phagocytosis, Autophagy, and bactericidal activity. Cell Rep. 2020;32(8):108079. https://doi.org/10.1016/j.celrep.2020.108079.
20. Haschka J, Englbrecht M, Hueber AJ, Manger B, Kleyer A, Reiser M, Finzel S, Tony HP, Kleinert S, Feuchtenberger M, Fleck M, Manger K, Ochs W, Schmitt-Haendle M, Wendler J, Schuch F, Ronneberger M, Lorenz HM, Nuesslein H, Alten R, Demary W, Henes J, Schett G, Rech J. Relapse rates in patients with rheumatoid arthritis in stable remission tapering or stopping antirheumatic therapy: interim results from the prospective randomised controlled RETRO

study. Ann Rheum Dis. 2016;75(1):45–51. https://doi.org/10.1136/annrheumdis-2014-206439.
21. Chen Z, Bozec A, Ramming A, Schett G. Anti-inflammatory and immune-regulatory cytokines in rheumatoid arthritis. Nat Rev Rheumatol. 2019;15(1):9–17. https://doi.org/10.1038/s41584-018-0109-2.
22. Redlich K, Smolen JS. Inflammatory bone loss: pathogenesis and therapeutic intervention. Nat Rev Drug Discov. 2012;11(3):234–50. https://doi.org/10.1038/nrd3669.
23. Croft AP, Campos J, Jansen K, Turner JD, Marshall J, Attar M, Savary L, Wehmeyer C, Naylor AJ, Kemble S, Begum J, Dürholz K, Perlman H, Barone F, McGettrick HM, Fearon DT, Wei K, Raychaudhuri S, Korsunsky I, Brenner MB, Coles M, Sansom SN, Filer A, Buckley CD. Distinct fibroblast subsets drive inflammation and damage in arthritis. Nature. 2019;570(7760):246–51. https://doi.org/10.1038/s41586-019-1263-7.
24. Zhang J, Wang H, Chen H, Li H, Xu P, Liu B, Zhang Q, Lv C, Song X. ATF3 -activated accelerating effect of LINC00941/lncIAPF on fibroblast-to-myofibroblast differentiation by blocking autophagy depending on ELAVL1/HuR in pulmonary fibrosis. Autophagy. 2022;18(11):2636–55. https://doi.org/10.1080/15548627.2022.2046448.
25. Mehta B, Goodman S, DiCarlo E, Jannat-Khah D, Gibbons JAB, Otero M, Donlin L, Pannellini T, Robinson WH, Sculco P, Figgie M, Rodriguez J, Kirschmann JM, Thompson J, Slater D, Frezza D, Xu Z, Wang F, Orange DE. Machine learning identification of thresholds to discriminate osteoarthritis and rheumatoid arthritis synovial inflammation. Arthritis Res Ther. 2023;25(1):31. https://doi.org/10.1186/s13075-023-03008-8.
26. Feng Q, Xia W, Wang S, Dai G, Jiao W, Guo N, Li H, Zhang G. Etodolac improves collagen induced rheumatoid arthritis in rats by inhibiting synovial inflammation, fibrosis and hyperplasia. Mol Biomed. 2021;2(1):33. https://doi.org/10.1186/s43556-021-00052-1.
27. Shkhyan R, Flynn C, Lamoure E, Sarkar A, Van Handel B, Li J, York J, Banks N, Van der Horst R, Liu NQ, Lee S, Bajaj P, Vadivel K, Harn HI, Tassey J, Lozito T, Lieberman JR, Chuong CM, Hurtig MS, Evseenko D. Inhibition of a signaling modality within the gp130 receptor enhances tissue regeneration and mitigates osteoarthritis. Sci Transl Med. 2023;15(688):eabq2395. https://doi.org/10.1126/scitranslmed.abq2395.
28. Kerschbaumer A, Sepriano A, Bergstra SA, Smolen JS, van der Heijde D, Caporali R, Edwards CJ, Verschueren P, de Souza S, Pope JE, Takeuchi T, Hyrich KL, Winthrop KL, Aletaha D, Stamm TA, Schoones JW, Landewé RBM. Efficacy of synthetic and biological DMARDs: a systematic literature review informing the 2022 update of the EULAR recommendations for the management of rheumatoid arthritis. Ann Rheum Dis. 2023;82(1):95–106. https://doi.org/10.1136/ard-2022-223365.
29. Onuora S. RA remission maintained after MTX withdrawal. Nat Rev Rheumatol. 2021;17(1):2. https://doi.org/10.1038/s41584-020-00554-2.
30. Gao X, Han Z, Huang C, Lei H, Li G, Chen L, Feng D, Zhou Z, Shi Q, Cheng L, Zhou X. An anti-inflammatory and neuroprotective biomimetic nanoplatform for repairing spinal cord injury. Bioact Mater. 2022;18:569–82. https://doi.org/10.1016/j.bioactmat.2022.05.026.
31. Ma Y, Lu Z, Jia B, Shi Y, Dong J, Jiang S, Li Z. DNA origami as a nanomedicine for targeted rheumatoid arthritis therapy through reactive oxygen species and nitric oxide scavenging. ACS Nano. 2022;16(8):12520–31. https://doi.org/10.1021/acsnano.2c03991.
32. Qiao H, Mei J, Yuan K, Zhang K, Zhou F, Tang T, Zhao J. Immune-regulating strategy against rheumatoid arthritis by inducing tolerogenic dendritic cells with modified zinc peroxide nanoparticles. J Nanobiotechnol. 2022;20(1):323. https://doi.org/10.1186/s12951-022-01536-0.
33. Qiao Q, Liu X, Yang T, Cui K, Kong L, Yang C, Zhang Z. Nanomedicine for acute respiratory distress syndrome: the latest application, targeting strategy, and rational design. Acta Pharm Sin B. 2021;11(10):3060–91. https://doi.org/10.1016/j.apsb.2021.04.023.
34. Pan W, Li Z, Qiu S, Dai C, Wu S, Zheng X, Guan M, Gao F. Octahedral Pt-MOF with au deposition for plasmonic effect and Schottky junction enhanced hydrogenothermal therapy of rheumatoid arthritis. Mater Today Bio. 2022;13:100214. https://doi.org/10.1016/j.mtbio.2022.100214.
35. Rahiman N, Markina YV, Kesharwani P, Johnston TP, Sahebkar A. Curcumin-based nanotechnology approaches and therapeutics in restoration of autoimmune diseases. J Control Release. 2022;348:264–86. https://doi.org/10.1016/j.jconrel.2022.05.046.
36. Zheng X, Yang H, Zhang Z, Liang X, Liu Y, Wang C, Yang X, Tang J, Mao J, Nie Y, Zhou X, Li C. pH-responsive size-adjustable liposomes induce apoptosis of fibroblasts and macrophages for rheumatoid arthritis treatment. Acta Biomater. 2024;179:256–71. https://doi.org/10.1016/j.actbio.2024.03.006.
37. Yang L, Sha Y, Wei Y, Fang H, Jiang J, Yin L, Zhong Z, Meng F. Mannose-mediated nanodelivery of methotrexate to macrophages augments rheumatoid arthritis therapy. Biomater Sci. 2023;11(6):2211–20. https://doi.org/10.1039/d2bm02072f.
38. Li J, Gong X. The Emerging Development of Multicolor Carbon dots. Small. 2022;18(51):e2205099. https://doi.org/10.1002/smll.202205099.
39. Ci Q, Wang Y, Wu B, Coy E, Li JJ, Jiang D, Zhang P, Wang G. Fe-Doped Carbon dots as NIR-II fluorescence probe for in vivo gastric imaging and pH detection. Adv Sci. 2023;10(7):e2206271. https://doi.org/10.1002/advs.202206271.
40. Wan J, Xu S, Li J, Yu M, Zhang K, Wei G, Su Z. Facile synthesis of multifunctional pharmaceutical carbon dots for targeted bioimaging and chemotherapy of tumors. Nanoscale. 2022;14(31):11359–68. https://doi.org/10.1039/d2nr03321f.
41. Zhao C, Wang X, Yu L, Wu L, Hao X, Liu Q, Lin L, Huang Z, Ruan Z, Weng S, Liu A, Lin X. Quaternized carbon quantum dots with broad-spectrum antibacterial activity for the treatment of wounds infected with mixed bacteria. Acta Biomater. 2022;138:528–44. https://doi.org/10.1016/j.actbio.2021.11.010.
42. Bai X, Zhang X, Xiao J, Lin X, Lin R, Zhang R, Deng X, Zhang M, Wei W, Lan B, Weng S, Chen M. Endowing polyetheretherketone with Anti-infection and Immunomodulatory Properties through Guanidination Carbon dots Modification to Promote Osseointegration in Diabetes with MRSA infection. Adv Healthc Mater. 2024;13(7):e2302873. https://doi.org/10.1002/adhm.202302873.
43. Zhang XT, Bai XX, Deng XQ, Peng K, Zheng ZF, Xiao JC, Zhang R, Huang ZJ, Huang JY, Chen M, Weng SH. Long-term antibacterial activity of guanidinium carbon dots without detectable resistance for the effective treatment of pneumonia caused by Gram-negative bacteria. Carbon. 2023;213:118229. https://doi.org/10.1016/j.carbon.2023.118229.
44. Zhang R, Miao CF, Lin XY, Lin RJ, Deng XQ, Huang JY, Wang Y, Xu Y, Weng SH, Chen M. Carbon dots efficiently promote vascularization for enhanced repairing of orthopedic diseases with diabetic mellitus based on nanocatalytic medicine. Carbon. 2024;217:118617. https://doi.org/10.1016/j.carbon.2023.118617.
45. Li D, Ruan G, Zhang Y, Zhao Y, Zhu Z, Ou Q, Huang H, Chen J, Han W, Tang S, Li J, Wang L, Chen T, Bai X, Cai D, Ding C. Metformin attenuates osteoarthritis by targeting chondrocytes, synovial macrophages and adipocytes. Rheumatology. 2023;62(4):1652–61. https://doi.org/10.1093/rheumatology/keac467.
46. Xue J, Li X, Liu P, Li K, Sha L, Yang X, Zhu L, Wang Z, Dong Y, Zhang L, Lei H, Zhang X, Dong X, Wang H. Inulin and metformin ameliorate polycystic ovary syndrome via anti-inflammation and modulating gut microbiota in mice. Endocr J. 2019;66(10):859–70. https://doi.org/10.1507/endocrj.EJ18-0567.
47. Leng T, Wang Y, Cheng W, Wang W, Qu X, Lei B. Bioactive anti-inflammatory antibacterial metformin-contained hydrogel dressing accelerating wound healing. Biomater Adv. 2022;135:212737. https://doi.org/10.1016/j.bioadv.2022.212737.
48. Arul V, Chandrasekaran P, Sethuraman MG. Reduction of Congo Red using nitrogen doped fluorescent carbon nanodots obtained from sprout extract of *Borassus flabellifer*. Chem Phys Lett. 2020;754:137646. https://doi.org/10.1016/j.cplett.2020.137646.
49. Tammina SK, Wan Y, Li Y, Yang Y. Synthesis of N, Zn-doped carbon dots for the detection of Fe^{3+} ions and bactericidal activity against Escherichia coli and Staphylococcus aureus. J Photochem Photobiol B. 2020;202:111734. https://doi.org/10.1016/j.jphotobiol.2019.111734.
50. Wang X, Zhao L, Hu JS, Wei H, Liu XY, Li ES, Yang SH. Rational design of novel carbon-oxygen quantum dots for ratiometrically mapping pH and reactive oxygen species scavenging. Carbon. 2022;190:115–24. https://doi.org/10.1016/j.carbon.2022.01.006.
51. Yan F, Yi C, Sun J, Zang Y, Wang Y, Xu M, Xu J. Self-quenching-resistant solid-state carbon dots for mechanism and applications. Microchim Acta. 2021;188(12):412. https://doi.org/10.1007/s00604-021-05068-6.
52. Chen YY, Wang ZZ, Hao XL, Li FL, Zheng YJ, Zhang JZ, Lin XH, Weng SH. Selective and sensitive fluorescent monitoring of acid phosphatase (ACP) activity under neutral conditions through the ACP enzymatic catalysis of dopamine as a new substrate to polydopamine, Sens. Actuator B-Chem. 2019;297:126784. https://doi.org/10.1016/j.snb.2019.126784.
53. Han Y, Tang B, Wang L, Bao H, Lu Y, Guan C, Zhang L, Le M, Liu Z, Wu M. Machine-learning-driven synthesis of Carbon dots with enhanced Quantum yields. ACS Nano. 2020;14(11):14761–8. https://doi.org/10.1021/acsnano.0c01899.
54. Ye Z, Wei L, Geng X, Wang X, Li Z, Xiao L. Mitochondrion-Specific blinking fluorescent bioprobe for nanoscopic monitoring of Mitophagy. ACS Nano. 2019;13(10):11593–602. https://doi.org/10.1021/acsnano.9b05354.

55. Mousavi-Koodehi B, Darzi L, Sadeghizadeh M, Najafi F, Forouzandeh-Moghdam M. Replacement of hydrochloride in metformin hydrochloride with caprylic acid to investigate its effects on MCF-7 and MDA-MB-231 breast cancer cell lines. Life Sci. 2022;293:120308. https://doi.org/10.1016/j.lfs.2022.120308.
56. Xu Y, Wang B, Zhang M, Zhang J, Li Y, Jia P, Zhang H, Duan L, Li Y, Li Y, Qu X, Wang S, Liu D, Zhou W, Zhao H, Zhang H, Chen L, An X, Lu S, Zhang S. Carbon dots as a potential therapeutic Agent for the treatment of Cancer-related Anemia. Adv Mater. 2022;34(19):e2200905. https://doi.org/10.1002/adma.202200905.
57. Xue Y, Nestor G. Determination of Amide cis/trans isomers in N-Acetyl-d-glucosamine: tailored NMR analysis of the N-Acetyl Group Conformation. ChemBioChem. 2022;23(17):e202200338. https://doi.org/10.1002/cbic.202200338.
58. Sadeghi M, Haghshenas B, Nami Y. Bifidobacterium exopolysaccharides: new insights into engineering strategies, physicochemical functions, and immunomodulatory effects on host health. Front Microbiol. 2024;15:1396308. https://doi.org/10.3389/fmicb.2024.1396308.
59. Hu X, Zhao S, Li F, Zhang X, Pan Y, Lu J, Li Y, Bao M. The structure, characterization and immunomodulatory potential of exopolysaccharide produced by Planococcus rifietoensis AP-5 from deep-sea sediments of the Northwest Pacific. Int J Biol Macromol. 2023;245:125452. https://doi.org/10.1016/j.ijbiomac.2023.125452.
60. Wang R, Yao Y, Gao Y, Liu M, Yu Q, Song X, Han X, Niu D, Jiang L. CD133-Targeted hybrid nanovesicles for Fluorescent/Ultrasonic imaging-guided HIFU Pancreatic Cancer Therapy. Int J Nanomed. 2023;18:2539–52. https://doi.org/10.2147/ijn.S391382.
61. Xin Li J, Jiao Zhang M, Feng Shi J, Wang SP, Mei Zhong X, Han Wu Y, Qu Y, Le Gao H, Zhang JM. pH-sensitive nano-polyelectrolyte complexes with arthritic macrophage-targeting delivery of triptolide. Int J Pharm. 2023;632:122572. https://doi.org/10.1016/j.ijpharm.2022.122572.
62. Shen X, Yang Z, Dai X, Feng W, Li P, Chen Y. Calcium Hexacyanoferrate Nanozyme enhances plant stress resistance by oxidative stress alleviation and heavy metal removal. Adv Mater. 2024;36(30):e2402745. https://doi.org/10.1002/adma.202402745.
63. Bauer B, Chyou PH, Stratman EJ, Green C. Noninvasive testing for nonalcoholic steatohepatitis and hepatic fibrosis in patients with psoriasis receiving long-term Methotrexate Sodium Therapy. JAMA Dermatol. 2017;153(10):977–82. https://doi.org/10.1001/jamadermatol.2017.2083.
64. Tang Z, Meng S, Yang X, Xiao Y, Wang W, Liu Y, Wu K, Zhang X, Guo H, Zhu YZ, Wang X. Neutrophil-Mimetic, ROS Responsive, and Oxygen Generating nanovesicles for targeted interventions of refractory rheumatoid arthritis. Small. 2024;20(20):e2307379. https://doi.org/10.1002/smll.202307379.
65. Liu X, Chen X, Zhang C, Huang M, Yu H, Wang Y, Wang Y. Mitochondrion-NLRP3 inflammasome activation in macrophages: a novel mechanism of the anti-inflammatory effect of Notopterygium in rheumatoid arthritis treatment. Biomed Pharmacother. 2023;167:115560. https://doi.org/10.1016/j.biopha.2023.115560.
66. Meyer A, Zack SR, Nijim W, Burgos A, Patel V, Zanotti B, Volin MV, Amin MA, Lewis MJ, Pitzalis C, Arami S, Karam JA, Sweiss NJ, Shahrara S. Metabolic reprogramming by Syntenin-1 directs RA FLS and endothelial cell-mediated inflammation and angiogenesis. Cell Mol Immunol. 2024;21(1):33–46. https://doi.org/10.1038/s41423-023-01108-8.
67. Hibi M, Murakami M, Saito M, Hirano T, Taga T, Kishimoto T. Molecular cloning and expression of an IL-6 signal transducer, gp130. Cell. 1990;63(6):1149–57. https://doi.org/10.1016/0092-8674(90)90411-7.
68. Poggioli R, Hirani K, Jogani VG, Ricordi C. Modulation of inflammation and immunity by omega-3 fatty acids: a possible role for prevention and to halt disease progression in autoimmune, viral, and age-related disorders. Eur Rev Med Pharmacol Sci. 2023;27(15):7380–400. https://doi.org/10.26355/eurrev_202308_33310.
69. O'Neil LJ, Oliveira CB, Wang X, Navarrete M, Barrera-Vargas A, Merayo-Chalico J, Aljahdali R, Aguirre-Aguilar E, Carlucci P, Kaplan MJ, Carmona-Rivera C. Neutrophil extracellular trap-associated carbamylation and histones trigger osteoclast formation in rheumatoid arthritis. Ann Rheum Dis. 2023;82(5):630–8. https://doi.org/10.1136/ard-2022-223568.
70. Lee S, Choi E, Chae S, Koh JH, Choi Y, Kim JG, Yoo SA, Hwang D, Kim WU. Identification of MYH9 as a key regulator for synoviocyte migration and invasion through secretome profiling. Ann Rheum Dis. 2023;82(8):1035–48. https://doi.org/10.1136/ard-2022-223625.
71. Prasad P, Verma S, Surbhi NK, Ganguly V, Chaturvedi SA, Mittal. Rheumatoid arthritis: advances in treatment strategies. Mol Cell Biochem. 2023;478(1):69–88. https://doi.org/10.1007/s11010-022-04492-3.
72. Angela S, Fadhilah G, Hsiao WW, Lin HY, Ko J, Lu SC, Lee CC, Chang YS, Lin CY, Chang HC, Chiang WH. Nanomaterials in the treatment and diagnosis of rheumatoid arthritis: Advanced approaches. SLAS Technol. 2024;29(4):100146. https://doi.org/10.1016/j.slast.2024.100146.
73. Han H, Xing J, Chen W, Jia J, Li Q. Fluorinated polyamidoamine dendrimer-mediated miR-23b delivery for the treatment of experimental rheumatoid arthritis in rats. Nat Commun. 2023;14(1):944. https://doi.org/10.1038/s41467-023-36625-7.
74. Guan J, Tan X, Jiao J, Lai S, Zhang H, Kan Q, He Z, Sun M, Sun J. Iron ion-coordinated carrier-free supramolecular co-nanoassemblies of dual DNA topoisomerase-targeting inhibitors for tumor suppression. Acta Biomater. 2022;144:121–31. https://doi.org/10.1016/j.actbio.2022.03.027.
75. Guo D, Shi C, Wang L, Ji X, Zhang S, Luo J. A rationally designed Micellar Nanocarrier for the delivery of hydrophilic methotrexate in Psoriasis Treatment. ACS Appl Bio Mater. 2020;3(8):4832–46. https://doi.org/10.1021/acsabm.0c00342.
76. Lei Y, Zhang Q, Kuang G, Wang X, Fan Q, Ye F. Functional biomaterials for osteoarthritis treatment: from research to application. Smart Med. 2022;1(1):e20220014. https://doi.org/10.1002/smmd.20220014.
77. Zhou Y, He H, Ding L, Wang T, Liu X, Zhang M, Zhang A, Fu J. Effects of gene polymorphisms on delayed MTX clearance, toxicity, and metabolomic changes after HD-MTX treatment in children with acute lymphoblastic leukemia. Eur J Pediatr. 2024;183(2):581–90. https://doi.org/10.1007/s00431-023-05267-8.
78. Honma T, Onda K, Masuyama K. Drug-drug interaction assessment based on a large-scale spontaneous reporting system for hepato- and renal-toxicity, and thrombocytopenia with concomitant low-dose methotrexate and analgesics use. BMC Pharmacol Toxicol. 2024;25(1):13. https://doi.org/10.1186/s40360-024-00738-6.
79. Farshidfar N, Fooladi S, Nematollahi MH, Iravani S. Carbon dots with tissue engineering and regenerative medicine applications. RSC Adv. 2023;13(21):14517–29. https://doi.org/10.1039/d3ra02336b.
80. Wang P, Yang N, Luo Y, Wang G, Zhou S, Huang S, Chen L, Zhao Y. Silymarin modified polysulfone hollow fiber membranes with antioxidant, anti-M1 macrophage polarization and hemocompatibility for blood purification. J Biomed Mater Res B Appl Biomater. 2023;111(10):1785–99. https://doi.org/10.1002/jbm.b.35285.
81. Sawoo R, Dey R, Ghosh R, Bishayi B. Exogenous IL-10 posttreatment along with TLR4 and TNFR1 blockade improves tissue antioxidant status by modulating sepsis-induced macrophage polarization. J Appl Toxicol. 2023;43(10):1549–72. https://doi.org/10.1002/jat.4496.
82. Han Z, Gao X, Wang Y, Cheng S, Zhong X, Xu Y, Zhou X, Zhang Z, Liu Z, Cheng L. Ultrasmall iron-quercetin metal natural product nanocomplex with antioxidant and macrophage regulation in rheumatoid arthritis. Acta Pharm Sin B. 2023;13(4):1726–39. https://doi.org/10.1016/j.apsb.2022.11.020.
83. Nygaard G, Firestein GS. Restoring synovial homeostasis in rheumatoid arthritis by targeting fibroblast-like synoviocytes. Nat Rev Rheumatol. 2020;16(6):316–33. https://doi.org/10.1038/s41584-020-0413-5.
84. Wu Z, Ma D, Yang H, Gao J, Zhang G, Xu K, Zhang L. Fibroblast-like synoviocytes in rheumatoid arthritis: surface markers and phenotypes. Int Immunopharmacol. 2021;93:107392. https://doi.org/10.1016/j.intimp.2021.107392.
85. Zhao Z, He S, Yu X, Lai X, Tang S, Mariya ME, Wang M, Yan H, Huang X, Zeng S, Zha D. Analysis and experimental validation of Rheumatoid Arthritis Innate Immunity Gene CYFIP2 and pan-cancer. Front Immunol. 2022;13:954848. https://doi.org/10.3389/fimmu.2022.954848.
86. Salnikova DI, Nikiforov NG, Postnov AY, Orekhov AN. Target Role of monocytes as Key cells of Innate Immunity in Rheumatoid Arthritis. Diseases. 2024;12(5):81. https://doi.org/10.3390/diseases12050081.
87. Shegarfi H, Naddafi F, Mirshafiey A. Natural killer cells and their role in rheumatoid arthritis: friend or foe? Sci World J. 2012;2012:491974. https://doi.org/10.1100/2012/491974.
88. Zhou S, Lu H, Xiong M. Identifying Immune Cell infiltration and effective diagnostic biomarkers in rheumatoid arthritis by Bioinformatics Analysis. Front Immunol. 2021;12:726747. https://doi.org/10.3389/fimmu.2021.726747.

89. Yamada S, Nagafuchi Y, Wang M, Ota M, Hatano H, Takeshima Y, Okubo M, Kobayashi S, Sugimori Y, Masahiro N, Yoshida R, Hanata N, Suwa Y, Tsuchida Y, Iwasaki Y, Sumitomo S, Kubo K, Shimane K, Setoguchi K, Azuma T, Kanda H, Shoda H, Zhang X, Yamamoto K, Ishigaki K, Okamura T, Fujio K. Immunomics analysis of rheumatoid arthritis identified precursor dendritic cells as a key cell subset of treatment resistance. Ann Rheum Dis. 2023;82(6):809–19. https://doi.org/10.1136/ard-2022-223645.

Publisher's note